國立交通大學

應用化學系

碩 士 論 文

連續波及飛秒脈衝雷射應用於微米至奈米大小球狀物質的光學捕捉

Optical Trapping Dynamics of Micron- to Nanometer-Sized Spherical Target Materials by Continuous Wave- and Femtosecond Pulse-Mode Laser Beams

研究生：江威逸

指導教授：增原 宏 教授

中華民國一百零一年七月

連續波及飛秒脈衝雷射應用於微米至奈米大小球狀物質的光學捕捉

Optical Trapping Dynamics of Micron- to Nanometer-Sized Spherical Target Materials by Continuous Wave- and Femtosecond Pulse-Mode Laser Beams

研究生：江威逸　　Student: Wei-Yi CHIANG

指導教授：增原 宏 教授　　Advisor: Prof. Dr. Hiroshi MASUHARA

A Thesis
Submitted to M. S. Program
Department of Applied Chemistry
College of Science
National Chiao Tung University
in Partial Fulfillment of the Requirements
for the Degree of
Master
in

Applied Chemistry

July 2012

Hsinchu, Taiwan, Republic of China

中華民國一百零一年七月

Published paper

Anwar Usman, **Wei-Yi Chiang**, Hiroshi Masuhara, Optical trapping and polarization-controlled scattering of dielectric spherical nanoparticles by femtosecond laser pulses, J. Photochem. Photobiol. A: Chemistry 234 (2012) 83-90.

Published proceeding

Anwar Usman, **Wei-Yi Chiang**, Hiroshi Masuhara, Laser Trapping-Induced Reconfiguration of Individual Smectic Liquid Crystal Micro-Droplet Showing Size-Dependent Dynamics, Proc. SPIE 8274 (2012) 82740L1-8.

Conference

1. "Orientation Modulation in Individually Trapped Liquid Crystal Droplets by Tightly Focused Laser Beam",
   Wei-Yi Chiang, Anwar Usman, Takayuki Uwada, Hiroshi Masuhara,
   2011 Spring Symposium of Photochemistry Association in Taiwan, 15 - 16 February, 2011, Hsinchu, Taiwan
2. "Orientation Modulation in Individually Trapped Liquid Crystal Droplets by Tightly Focused Laser Beam",
   Wei-Yi Chiang, Anwar Usman, Takayuki Uwada, Hiroshi Masuhara,
   The 3rd Workshop on Laser Bio/Nano Science, 4th March, 2011, Hsinchu, Taiwan
3. "Size-dependent phase modulation of individually trapped liquid crystal micro-droplets",
   Wei-Yi Chiang, Anwar Usman, Hiroshi Masuhara,
   2011 年光化学討論会, 6-8 September, 2011, Miyasaki, Japan
4. "Size-dependent phase modulation of individually trapped liquid crystal micro-droplets",
   Wei-Yi Chiang, Anwar Usman, Hiroshi Masuhara,
   Japan-Taiwan joint workshop: Future Perspective on NanoBio Science Pioneered by Light, 4th Octorber, 2011, Hsinchu, Taiwan
5. "Femtosecond Laser Pulse-Induced Optical Trapping and Polarization-Controlled Off-Axis Scattering of Dielectric Spherical Nanoparticles",
   Wei-Yi Chiang, Anwar Usman, Hiroshi Masuhara,
   2012 Spring Symposium of Photochemistry Association in Taiwan, 9-10 February, 2012, Kaohsiung, Taiwan
6. "Concentration Dependence of Polarization-Controlled Scattering of Polystyrene Nanoparticles by Femtosecond Laser Pulses",
   Wei-Yi Chiang, Anwar Usman, Takayuki Uwada, Hiroshi Masuhara,

応用物理学関係連合講演会, 15-18 March, 2012, Tokyo, Japan

7. “Axial Field-Controlled Direction of Scattered Dielectric Spherical Nanoparticles in Optical Trapping”,
   Anwar Usman, **Wei-Yi Chiang**, Hiroshi Masuhara,
   2012 Spring Symposium of Photochemistry Association in Taiwan, 9-10 February, 2012, Kaohsiung, Taiwan
8. “Dynamic Optical Force Exerting on Dielectric Nanoparticles by Femtosecond Laser Pulses, Leading to Polarization-Controlled Off-Axis Scattering”,
   Anwar Usman, **Wei-Yi Chiang**, Hiroshi Masuhara,
   応用物理学関係連合講演会, 15-18 March, 2012, Tokyo, Japan
9. “Femtosecond Laser-Induced Trapping and Off-Axis Ejection of Dielectric Spherical Nanoparticles”,
   Anwar Usman, **Wei-Yi Chiang**, Hiroshi Masuhara,
   The 1st Workshop on Laser Trapping with Laser BioNano Science, 4-6 April, 2012, Hsinchu, Taiwan
10. “Laser Trapping-Induced Reconfiguration of Individual Smectic Liquid Crystal Micro-Droplet Showing Size-Dependent Dynamics”,
    Anwar Usman, **Wei-Yi Chiang**, Takayuki Uwada, Hiroshi Masuhara,
    SPIE photonic west, 22-28 January, 2012, San Francisco, USA

連續波及飛秒脈衝雷射應用於微米至奈米大小球狀物質的光學捕捉

研究生：江威逸　　指導教授：增原宏 教授

國立交通大學 應用化學系碩士班

摘要

微奈米結構有機物或聚合物的光學捕捉提供光學調控分子排列以及聚焦雷射產生動態變化的資訊。這篇論文含蓋了兩個方向，分別是藉由聚焦連續波雷射光學捕捉引發微米大小液晶液珠內的分子排列以及飛秒雷射照射在 50 奈米大小的聚苯乙烯球所產生的動態變化。

我們探討在聚焦連續波雷射照射下液晶液珠內的分子重排而重排發生自內部並遍及整個液珠，且相轉變的門檻能量隨液珠大小而改變。我們認為當焦點體積內的光學重組克服液珠的介面錨定效應便會產生重排。藉由探討電場對液晶液珠的作用能以及引入液珠介面錨定效應的概念，我們成功建立了可解釋隨液珠大小而產生不同變化的模型。

飛秒脈衝雷射照射在 50 奈米大小聚苯乙烯球的動態變化呈現出極化方向控制的兩個相反方向並交互變換的散射且與雷射極化方向相互垂直。由於光電場和極化介電球誘導偶極矩之間的相互作用，我們重新討論作用在介電奈米球體上的勞倫茲力用以解釋新現象的發生。我們考慮高數值孔徑物鏡產生的軸向及橫向電場導出軸向電場是散射力及時間變化力橫向組成的原因並且控制雷利粒子散射的方向。透過這些發現，我們提供了聚焦超快雷射脈衝雷利粒子動態光學捕捉很重要的資訊。

Optical Trapping Dynamics of Micron- to Nanometer-Sized Spherical Target Materials by Continuous Wave- and Femtosecond Pulse-Mode Laser Beams

Student: Wei-Yi CHIANG Advisor: Prof. Dr. Hiroshi MASUHARA

M. S. Program, Department of Applied Chemistry
National Chiao Tung University

Abstract

Optical trapping of organic or polymeric micro- and nano-structures provides information on how their molecular configuration is optically manipulated or how their dynamical motions are controlled by the focused laser beam. This thesis covers both ideas of optical trapping-induced molecular configuration in micro-sized individual 4'-n-pentyl-4-cyanobiphenyl liquid crystalline droplets by tightly focused continues wave laser beam and dynamical motions of 50-nm-sized polystyrene beads by femtosecond pulsed laser beam.

We explore the reconfiguration in liquid crystal droplet under the irradiation of tightly focused cw laser beam. We show that reconfiguration took place throughout the inside of droplet, and the threshold power of the phase transition depends on droplet size. We propose that the droplet reconfiguration takes place when optical reorientation at the focal volume overcomes the droplet-liquid interfacial anchoring effect. By considering interaction energy of liquid crystal droplet by electric field and introducing liquid crystal droplet interfacial anchoring effect, we succeeded in building a model which can indicate the

dynamic change depending on size.

The dynamic motions of the 50 nm-sized polystyrene beads impinged by femtosecond pulsed laser beams show the polarization-controlled scattering in two opposite directions, in alternating manner, perpendicular to the laser polarization. To understand this new phenomenon we reconsider Lorentz force acting on a dielectric spherical nanoparticle due to interactions between light electric field and induced dipole moment of the polarizable dielectric sphere. We take axial and lateral electric fields into account produced by high numerical aperture objective lens. The axial electric field is responsible for lateral components of the scattering and temporal forces, and hence, controls the scattering directions of the Rayleigh particles. These findings provide important information about the dynamic optical trapping of the Rayleigh particles by highly focused ultrashort laser pulses.

Acknowledgment

Two years ago when I joined this laboratory I was worry with the new environment and unfamiliar people. Specially, all of the professors in this laboratory come from other countries, so I need to communicate in English, which is not familiar language for me, with them. Fortunately, even though my poor English, all of the professors have nice patience to listen and teach me.

Now, upon completing this thesis, I would like to express my gratitude to whom that have helped me in this two years. Particularly, I am deeply indebted to my supervisors Prof. Hiroshi Masuhara and Dr. Anwar Usman who supervise, advice, and encourage me to perform my research works and to write this thesis.

I also want to express my appreciation to Prof. Atsushi Miura, Prof. Takayuki Uwada, and Dr. Kenichi Yuyama who gave me helps, supports, and suggestions during my research works.

Additionally, I am obliged to acknowledge to my reviewers Prof. Hiroshi Masuhara, Prof. Atsushi Miura, Prof. Yen-Ju Cheng and Prof. Yoshiaki Teranishi for their kind evaluation on my thesis and permission to get the Master degree.

In this occasion, I also want to thank my seniors, Ping-Yu Hee, Jing-Ru Tu, Chung-Wei Huang and Tsung-Han Liu; classmates, Shun-Fa Wang, Ching-Hsu Tseng, Yan-Hua Huang, Tsu-Wei Hsu, Ling-Ting Huang; and junior, Chi-Shuin Wu for support,

encouraging, and help during these two years of laboratory life.

Besides, I want to thank the Department of Applied Chemistry of National Chiao Tung University for providing excellent environment and resource to do the research works.

Contents

List of Figures

CHAPTER 1

Introduction

The interactions of light with matter result in many fascinating phenomena. Over a long history of investigation of such interactions, the researches nowadays have arrived at nanometer scale of target material, a dimension much smaller than the wavelength of utilized light. One of the fascinating ideas in optics is the use of light to trap atoms and small particles [1,2]. This so called optical tweezers or optical trapping technique has already proven to be an essential tool in physics, biology, and chemistry [3,4]. Among the interesting applications of this technique in fabrication and characterization at the nanoscale [5], in such a thriving field of research over the past 40 years the laser trapping-induced crystallization of amino acids has generated attentions as a model for three-dimensional molecular rearrangement by focused laser beam [6-10]. The basic concept of the optical trapping is the generation of gradient force, as illustrated in Figure 1.1 that the incident light is refracted through the particle, leading to the change of momentum of the photons. According to the conservation of momentum, a gradient force is exerted on the particle in the direction to the beam center [11].

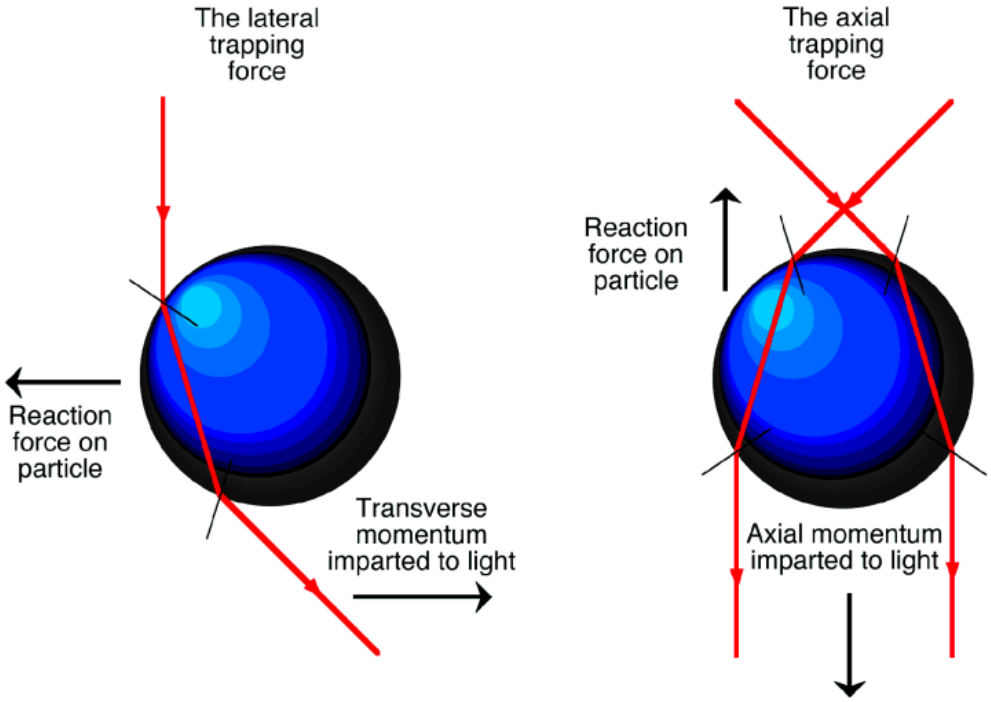

Figure 1.1 The optical forces acting on particle performed by momentum transfer of photons**.**

This thesis attempts to understand molecular reconfiguration inside microparticles trapped by focused laser beam as well as to explore the novel trapping phenomena of nanoparticles by ultrafast laser pulses. For the earlier attempt, liquid crystal droplets with soft and reconfigurable molecular organization properties were used as the target material optically trapped by continuous wave-mode laser beam. Though the researches on the liquid crystal droplets by focused beam have been started a few years ago, most researches employed the laser power and optical condition below those necessary to induce a laser trapping crystallization similarly to the amino acids [12-15]. Thus, in this work, the trapping behavior was studied in a wide range of laser power tightly focused by a high numerical objective lens. For the latter attempt, 50-nm-sized polystyrene beads suspended in water were

the target material, and femtosecond pulse-mode laser beam was used as the trapping beam substituting the traditional continuous wave laser. We note that in the beginning of ultrashort pulsed laser trapping was started, the laser pulse trapping was believed to be as just effective as cw laser trapping of microparticles in particular [16]. Indeed, when picosecond pulse-mode laser beam was finally shown to be able to trap less-than-5-nm sized CdTe quantum dots in 2007, optical trapping experiments with laser pulses started to attract more and more attention with many questions still to explore. More recently, research works on the ultrashort laser pulse-induced trapping behavior of nanoparticles provide several excellent phenomena, for instance, the control of crystalline properties and dimensions of nanodeposits of 25-nm-sized CdS particles [17] and the split of trapping site of gold NPs into two equivalent positions shifted from the focal center [18]. These findings highlight the advantages of pulse- over cw-mode laser beam in trapping ability and control on Rayleigh particles.

However, such fundamentally different behaviors of the three-dimensional optical trapping with the laser pulses to the cw laser also require theoretical elucidations, because the new phenomena are beyond the concept of conventional optical trapping. Thus, for a quantitative explanation we should rely upon the scattering theory of electromagnetic radiation, reexamining gradient, scattering, and temporal pulse-radiation forces, which are respectively related to spatial Lorentz force [19,20], momentum transfer from light to the dielectric NPs, and instantaneous Lorentz force throughout a pulse envelope. The scattering

cross section value of the nanoparticles was obtained based on Mie theory [21].

In Chapter 2 we describe the polarization- and droplet size-dependence of laser trapping-induced reconfiguration in individual radial symmetric liquid crystalline micro-droplets suspended in water. We found that the optical trapping of the droplet is indeed followed by a molecular reconfiguration, which takes place only when laser power density is above a definite threshold level. The relevant qualitative theoretical approximation is described based upon a likely mechanism of the molecular reconfiguration inside the droplet that involves local optical reorientation at focal volume when the interaction energy of liquid crystals with dielectric anisotropy aligned by the electric field of the focused laser beam exceeds Frank distortional energy. With this proposed mechanism, we show that the predicted dependence of the threshold power on the droplet size is in qualitative agreement with the experimental observation.

Chapter 3 discusses femtosecond laser pulse trapping behavior of polystyrene nanoparticles. The main focus of this chapter is laser pulse trapping behavior in comparison with the cw mode. We found that the laser pulses can trap a larger number of nanoparticles. In addition, the laser pulses induce nanoparticle flows out of the focal spot in two opposite directions, in an alternating manner, controlled by the laser polarization. We evaluate both gradient, scattering, and temporal forces by adopting Lorentz force of fundamental Gaussian beam exerted on Rayleigh particles, and by applying scattering cross section value of the

nanoparticles obtained based on Mie theory. We demonstrate that the lateral and axial electric fields produced by the high numerical aperture objective lens are responsible for the present novel phenomenon.

In Chapter 4 we conclude some important findings of the research works in this thesis, and provide the future outlooks of this research works, which already start to open new vistas for controlling the molecular reordering and reconfiguration of micro-droplets by the cw laser trapping, controlling dynamical motion of nanoparticle assembly by ultrafast laser pulses. The latter finding, in particular, is considered to be applicable for separation and sorting of nanoparticles with either different polarizabilities or scattering cross sections. Thus, the future research works will open more horizons and possible applications to be realistic.

References

[1] A. Ashkin, Phys. Rev. Lett. 24 (1970) 156..

[2] A. Ashkin, Proc. Natl. Acad. Sci. USA 94 (1997) 4853.

[3] K.C. Neuman, S.M. Block, Rev. Sci. Instrum. 75 (2004) 2787.

[4] K. Dholakia, P. Reece, M. Gu., Chem. Soc. Rev. 37 (2008) 42.

[5] E. Ozbay., Science 311 (2006), 189.

[6] T.Sugiyama, T. Adachi, H. Masuhara, Chem. Lett. 36 (2007) 1480.

[7] Y. Tsuboi, T. Shoji, N. Kitamura, J. Phys. Chem. C 114 (2010) 5589.

[8] T. Sugiyama, T. Adachi, H. Masuhara, Chem. Lett. 38 (2009) 482.

[9] T. Rungsimanon, K. Yuyama, T. Sugiyama, H. Masuhara, N. Tohnai, M. Miyata, J. Phys. Chem. Lett. 1 (2010) 599.

[10] T. Rungsimanon, K. Yuyama, T. Sugiyama, H. Masuhara, Cryst. Growth Des. 10 (2010) 4686.

[11] J.E. Molloy, M.J. Padgett, Contemp. Phys. 43 4 (2002) 241

[12] E. Brasselet, S. J. Joudkazis, Nonlinear Opt. Phys. Mater. 18 (2009) 167.

[13] N. Murazawa, S. Joudkazis, H. Misawa, Eur. Phys. J. E 20 (2006) 435.

[14] N. Murazawa, S. Joudkazis, S. Matsuo, H. Misawa, Small 1 (2005) 656.

[15] N. Murazawa, S. Joudkazis, H. Misawa, Opt. Express 14 (2006) 2481.

[16] B. Agate, C.T.A. Brown, W. Sibbett, K. Dholakia, Opt. Express 12 (2004) 3011.

[17] M. Sanz, R. de Nalda, J.F. Marco, J.G. Izquierdo, L. Banares, M. Castillejo, J. Phys. Chem. C 114 (2010) 4864

[18] Y. Jiang, T. Narushima, H. Okamoto, Nat. Phys. 6 (2010) 1005

[19] P. Bartlett, S. Henderson, J. Phys.: Condens. Matter 14 (2002) 7757

[20] Y. Harada, T. Asakura, Opt. Commun. 124 (1996) 529

[21] C.F. Bohren, D.R. Huffman, Absorption and Scattering of Light by Small Particles, Wiley, New York, 1983.

CHAPTER 2

Polarization and Droplet Size Dependences of Laser Trapping-Induced Reconfiguration in Individual Radial Symmetric Liquid Crystal Micro-Droplets

1. Introduction

Optical trapping technique utilizing a tightly focused continuous-wave (cw) laser beam allows one to manipulate micron- or a few tens of nm-sized objects with a high precision [1,2]. Therefore, this technique becomes indispensable and has been widely employed to control the deposition of dielectric particles [3,4], as well as to induce optical manipulation on single cells [5], polymers [6,7], micelles [8], J-aggregates [9], and amino acids [10,11]. In particular, the optical trapping of glycine, the simplest amino acid, dissolved in water leads to nucleation and growth of its single crystal [10,12] with its polymorphs being controllable by the laser power [13,14]. Such a three-dimensional molecular alignment accurately driven by a focused light is of interest for both fundamental sciences and applications. This finding also implies migration of molecules or clusters from the surrounding area to the focal spot as well as cooperative molecular realignment, and such effects have been demonstrated for gold nanoparticles and liquid crystal (LC) thin film by the focused laser beam [15-17].

The laser trapping-induced optical realignments have also been revealed in spherical LC droplets with various kinds of self-organized configurations depending on droplet-liquid boundary conditions in the medium they were dispersed [18-24]. Typically, the laser trapping beam can induce reconfiguration in radial nematic LC droplets, leading to conoscopic structures and spinning of the birefringent droplets due to angular momentum

transfer [20,23]. Similar phenomena were also observed for optically trapped bipolar nematic [18,19] or cholesteric LC droplets [21,22]. In the latter case, in particular, the rotation is accompanied by a distinct vertical motion of the droplet in the optical trap [21,22]. By contrast, at the similar level of laser power, molecular reconfiguration inside smectic LC droplets has never been observed, although the laser trapping beams can induce axial and lateral repositioning leading to wobbing rotation of the trapped droplets when the laser beam is circularly polarized [25]. Lamellar organization of LC molecules inside the droplets has been considered to induce large elastic rigidity, preventing the light-induced molecular reconfiguration inside the droplets [24,26]. Measuring rotation frequency of the optically trapped droplet and polarization change of the laser beam passed through the micro-sphere allow one to determine the viscosity of surrounding media precisely [27,28].

Recently, we have reported laser trapping behavior of radial symmetric 4'-pentyl-4-cyanobiphenyl (5CB) liquid crystalline micro-droplets dispersed in heavy water (D_2O) under highly focused near-infrared cw laser beam [29]. In our experiments, we found that the optical trapping of the radial symmetric droplet is indeed followed by a molecular reconfiguration, which takes place only when laser power density is above a definite threshold level. Here, we report in some detail a qualitative understanding of the experimentally observed reconfiguration by considering that the threshold and the dynamics of the reconfiguration depend on the droplet size and polarization state. The findings indicate that

likely mechanism of the molecular reconfiguration inside the smectic LC droplet involves local optical reorientation at focal volume when the interaction energy of LCs with dielectric anisotropy aligned by the electric field of the focused laser beam exceeds Frank distortional energy, followed by reconfiguration inside the confined droplet. With this mechanism, we show that the predicted dependence of the threshold power on the droplet size is in qualitative agreement with the experimental observation.

2. Experimental

2.1 Optical setup

The experimental setup is shown in Figure 2.1. A continuous wave (cw) 1064 nm Nd:YVO_4 laser beam (Spectra Physics; J20I-BL-106C) was focused into the sample cell, held on the stage of an inverted microscope (Olympus IX71). The beam was focused by an UPlanApo oil immersing objective lens (magnification 100 times and numerical aperture (N.A.) 1.35). After passing through the power adjustment, the laser beam was expanded and collimated to about 7 mm in diameter and the polarization state was controlled by a half-wave plate. After the objective lens, the laser power was operated in the range of 0.1-1.0 W, and the beam waist for 1064 nm was calculated to be 0.39 μm. The liquid crystal droplet reoriented by the highly focused laser beam was monitored conventionally by polarization optical microscopy (POM), which is composed by two orthogonal polarizers. From the top of the microscopy, visible probe light from a halogen lamp (λ=400-750 nm) was passed through a pair of polarizers and condenser lens, N.A. is 0.55, sandwiching the sample. The coupled charge-coupled device (CCD) camera (JAI; CV-A55IR E), running at 30 interlaced frames per second, was used to detect the transmittance probe light. The scattering light from near infrared was completely eliminated by low pass filter (LPF) before CCD camera.

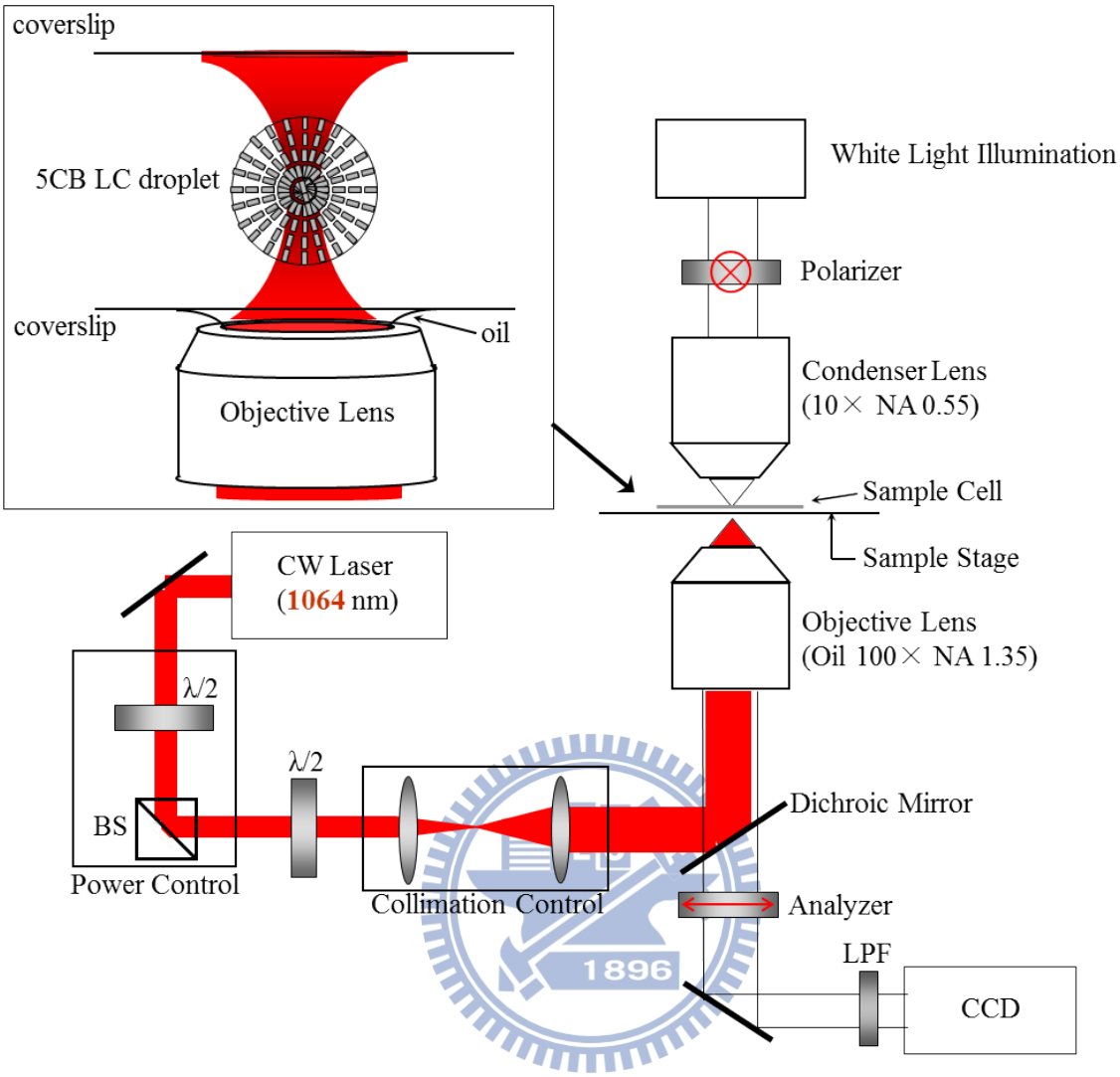

Figure 2.1 A schematic diagram of the experimental setup; BS = beam splitter, λ/2=half-wave plate, LPF = low pass filter with transmission edge at 900 nm. Inset: the cell containing an individually trapped smectic LC droplet by focused laser beam.

2.2 Sample preparation

The sample cell was prepared by two cover glasses (Matsunami; thickness 0.12-0.17 mm), and a chamber between the two cover glasses was formed by strips of parafilms along the glass edges with height 15-25 μm. The chamber was filled by 5CB (4-cyano-4'-pentylbiphenyl; 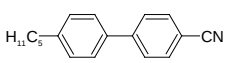) droplets (Tokyo Kasei Co.; the ordinary

and extraordinary refractive indices, n_o and n_e, are 1.54 and 1.74, respectively) suspended in D_2O without any additional surfactants. Comparing with H_2O, in this kind of condition, we can avoid temperature elevation induced by 1064 nm laser beam that has been reported to be 2.6 ºC/W and 24 ºC/W in H_2O [30,31]. Due to the interfacial tension, 5CB droplet always formed perfectly spherical and the diameter can be determined directly by POM image.

3 Results

3.1 Reconfiguration of the LC droplet

The diameter of the micro-droplets was within submicron to several microns. Due to their high refractive index, the droplets are highly polarizable and easily trapped by a steep optical-field gradient. In Figure 2.2 (a-b) are shown POM images for a ~2.5-μm-sized smectic droplet upon irradiation by linearly polarized laser beam with different laser power densities. We found that at low laser powers the droplet is optically trapped, so that its center is located at the focal area, its POM images show no time dependence, and the intrinsic lamellar configuration inside the droplet apparently remains intact. When the laser power was increased to few hundreds of MW/cm^2, we observed that the POM images of the optically trapped droplet are time-dependent. The images showed clearly that the radially symmetric configuration of the smectic droplet disappears, followed by the appearances of ring patterns of transmitted probe light passing through the trapped droplet. Typically, the ring patterns consisting of a small ring near the center and one or two larger concentric rings showed up clearly on time scales of seconds to a few tens of seconds depending on the laser power. Such time evolution of POM images indicate unambiguously that the radial symmetric droplet is reconfigured under the high power of laser trapping beam. In addition, we observed defocusing of the trapped droplet, as indicated by the change of droplet size in the

transmission images, though it is not so clearly observed for droplets with diameter less than 2 μm.

Figure 2.2 (c-e) shows the POM images for a ~3.5-μm-sized droplet trapped by circularly polarized laser beam with different laser power densities. Notably, for the small droplet, the circularly polarized laser trapping beam did not induce wobbing rotation. This suggests that optical trapping of the small droplet is on-center and it is consistent with the earlier report, in which off-center optical trapping is observed for smectic droplets larger than 4 μm in diameter independent on the laser power [25]. When we increased the laser power, the POM images show that the droplet was also trapped steadily at the early time of irradiation, and such a stable optical trap was followed by a wobbing rotation of the droplet around the trapping axis. The transition from the static to rotation states takes place in a few tens of milliseconds. In this case, once the droplet started to undergo a wobbing rotation, the rotation continues without stopping within our observation window of 90 s. Further increasing the laser power led a wobbing rotation to undergo temporarily. When such rotation stopped, the appearances of ring patterns similarly to those for a droplet trapped by the linearly polarized light were observed.

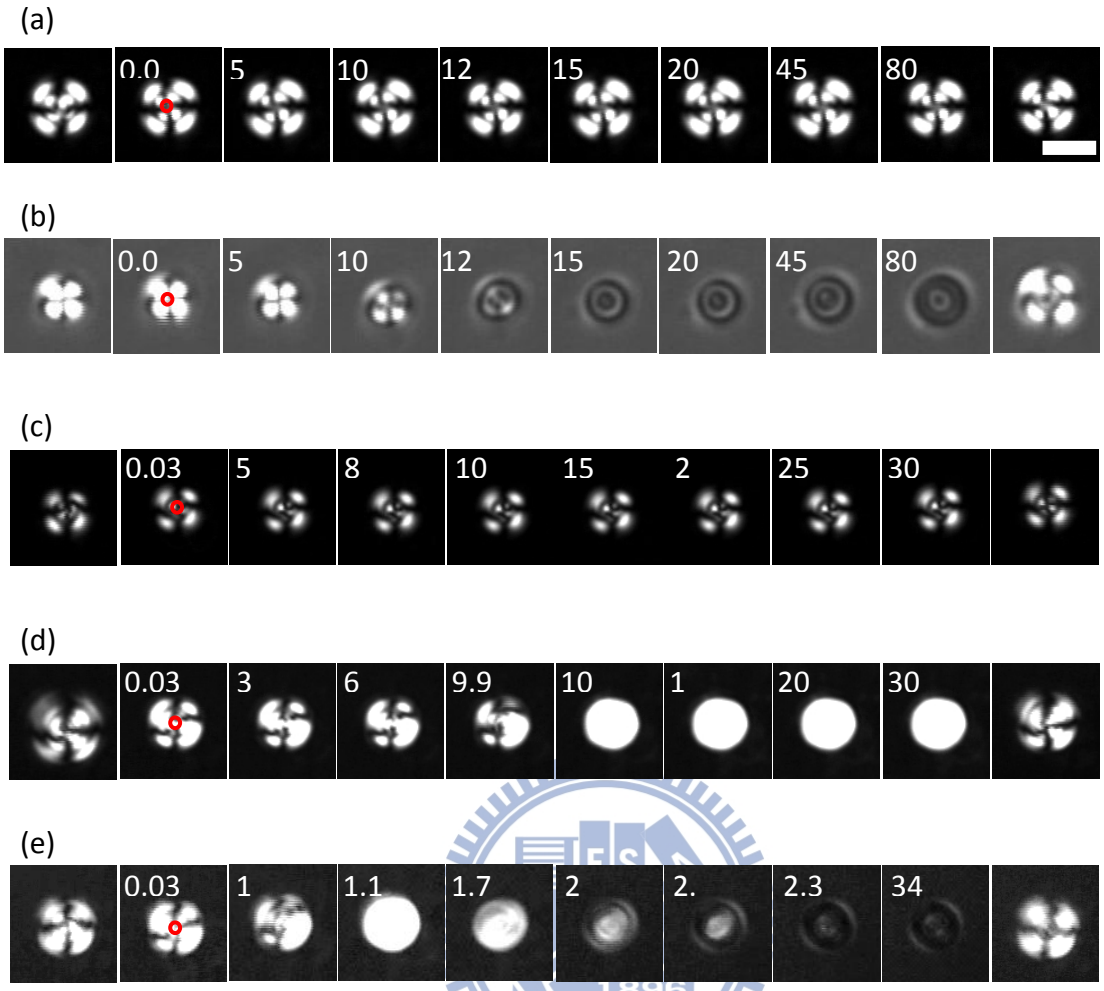

Figure 2.2 Sequences of time evolution of POM images of an individual smectic 5CB droplet optically trapped by a linearly polarized trapping beam at; (a) 130 mW (or 60 MW/cm^2); (b) 850 mW (or 360 MW/cm^2), and by a circularly polarized trapping beam at; (c) 130 mW (or 60 MW/cm^2), (d) 460 mW (or 190 MW/cm^2), and (e) 940 mW (or 390 MW/cm^2). The trapping time in second is indicated in each snapshot; while the most left and most right snapshot in each sequence is the image just before laser trapping beam is switched on and just after the beam is switched off, respectively. The red circles denote the focal spot area. The scale bar of 3 μm is applied for all images.

In addition to such polarization-dependent dynamics of the reconfiguration, increasing the laser power above the threshold led all the dynamics to be faster. When the laser beam was switched off, the transient ring patterns vanish immediately on the time scale of tens of milliseconds, restoring the initial radially symmetric pattern of a radial symmetric

droplet. Such an immediate restoration of the initial pattern, however, is independent on the laser power, and it is evidence for the existence of droplet-liquid interfacial anchoring effect as well as for the absences of optical memory, hysteresis, or storage effects.

3.2 Droplet size-dependence of threshold laser power

By varying the laser power to trap an individual LC droplet, we found that there is a clear threshold power, above which the optical trapping is followed by molecular reconfiguration throughout the inside of the droplet [29]. To evaluate the dependence of the threshold power on the droplet size and polarization state, we have performed and repeated the above process for different sizes of LC droplets for both linearly and circularly polarized beams. We found that the threshold is higher for a larger droplet. As far as the optical reconfiguration throughout the inside of the droplet as indicated by the formation of ring patterns is considered, we found that the threshold for circularly polarized laser beam tends to be slightly larger than that for linearly polarized beam. The droplet size and polarization dependences of the threshold trapping laser power to induce reconfiguration are shown in Figure 2.3.

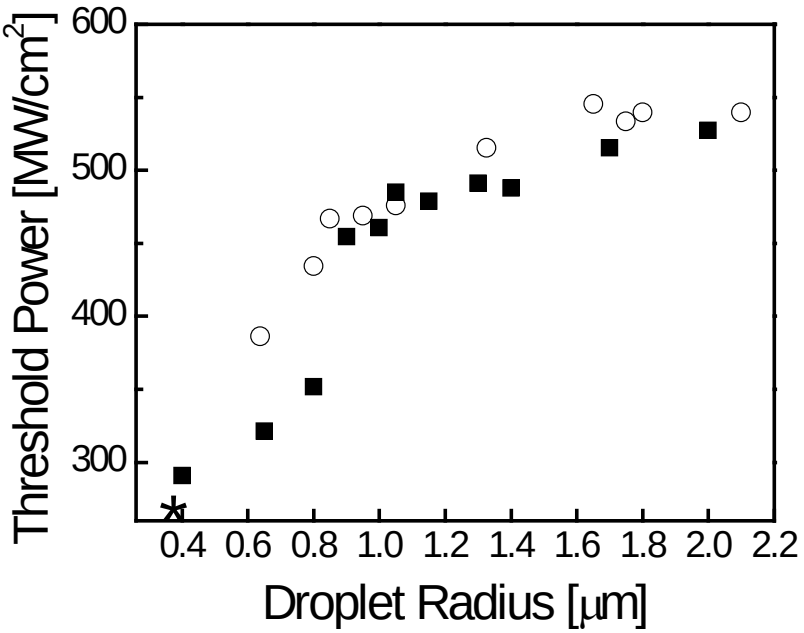

Figure 2.3 Plot of threshold laser power density to induce the phase transition as a function of droplet radius. The calculated beam waist is denoted by an asterisk. Data points denoted with filled rectangular and open circular are for linearly and circularly polarized beams, respectively.

4. Discussion

4.1 Laser trapping-induced reconfiguration

We should note that our observation on laser trapping properties of the radial symmetric 5CB droplet at low laser powers are in accordance with those recently reported and well documented in works by Murazawa *et al*. [25] and Brasselet *et al*. [24] Our important experimental finding is that, actually, optically induced reconfiguration does exist in the droplet under high laser powers with a sharp threshold, similarly to the cases of other LC droplets with radial configurations [23,32,33].

To interpret the optically-induced reconfiguration in the radial nematic LC droplet, we first consider optical reorientation of LCs, analogous to optical Fréedericksczc transition (OFT) in LC thin films. The optical reorientation should take place when the free-energy by the light field exceeds Frank distortional energy. In a corresponding LC thin slab analog, in which reorientation driven by optical nonlinearities has been accurately described, for conventional light irradiations, the threshold of light density to induce molecular reorientation, I_{th}, is given by [34,35]

$$I_{th} = \frac{\pi^2 cKn_e^2}{d^2 n_o (n_e^2 - n_o^2)} \qquad (2.1)$$

where c denotes the speed of light, d is the thickness of the LC film, n_e and n_o are the

extraordinary and ordinary refractive index, and K is the average Frank elastic constant. If one considers that the diameter of the droplet is approximately equal with the thickness of the LC thin slab analog, with $K \cong 10$ pN, Eqn. (1) gives the threshold light density for a droplet of 2.5-μm-diameter to be approximately 2 MW/cm^2, corresponding to electric field strength of 2 V/μm. This calculated threshold power, however, is about two orders of magnitude lower than the actual power to induce the reconfiguration throughout the inside of the droplet (the threshold power density is ~360 MW/cm^2). The striking difference between the calculation and experimental value is due to that laser intensity of a focused beam is steeply distributed around the diffraction limited size, not all inside the droplet volume. Nevertheless, with this calculation, we proposed that the focused beam with laser powers slightly above OFT threshold should not only generate gradient force, which confines stably the birefringent droplet, but such a polarized laser beam propagating in the confined droplet can also induce optical reorientation locally within the focal spot at the droplet center, although such local reorientation is too small inside the droplet to be detected by the POM imaging.

As a self-organized structure, droplet-liquid interface energetic will also control the molecular orientation inside the droplet through the interfacial anchoring effect. In this sense, the interface can be considered to act as the anchoring layer. Under the optical trapping at laser powers between the OFT and reconfiguration threshold, the reorientation propagates from the focal spot to the close vicinity area through most probably cooperative effects, and

thus, the droplet may adopt a kind of intermediate configuration. In this situation, the local reorientations inside the droplet will induce non-symmetrical orientations, and such symmetry breaking inside the droplet leads to spatially unequal torque. This is clearly indicated by rotation of the droplet under circularly polarized beam. At higher powers, when optical reorientation overcomes the anchoring effect, rotation of the droplet is coupled with its reconfiguration. Thus, the rotation is induced as the result of local optical reorientations and it can be considered as an early process or precursor of the reconfiguration, which most probably is an equilibrium reorientation throughout the inside of the droplet. This means that, when such an equilibrium configuration is formed, the local birefringence ultimately becomes negligible, the torque is spatially balanced, and the rotation stops as observed with the appearances of ring patterns.

The ring patterns of the optical transmission can be usually related to a far-field intensity distribution of the transmitted light due to its spatial self-phase modulation and the wave-front curvature, when the light passes through the nematic LC thin film [36,37]. In this droplet case, the ring patterns may indicate that, in the equilibrium state, the LC molecules inside the droplet is reoriented, but since both linearly and circularly polarized beams result in the same POM images of the reconfigured droplet, we could draw a conclusion that their LC orientations are not preferred along the laser polarization. This is an indication that reconfiguration is not solely due to the laser polarization in the focal spot, but also involves

cooperative effects throughout the inside of the droplet. Though the LC molecular configuration inside the droplet is still an open question, we qualitatively interpreted that one of possible structures is a kind of twisted configuration [29]. However, as the initial pattern is immediately restored when the laser beam is switched off, we could consider that the molecular alignment at the interfacial layer which acts as an anchoring surface should always remain intact.

Upon the reconfiguration, the local refractive index inside the droplet should jump between the extraordinary and ordinary refractive indices. As a consequence, the optical forces exerting on the droplet should be also modified, resulting in a relocation of the droplet slightly from the initial trapping center. This could be attributable to the change in droplet diameter in the POM image. In comparison, the similar effect has been observed in photo-induced molecular reorganization inside optically trapped cholesteric LC droplets [21,22].

4.2 A proposed model mechanism for droplet size dependence of threshold power

Considering that the reconfiguration is initially induced and started by the optical reorientation at the focal spot, the droplet size (a) with respect to the beam waist (r_0) should

be the key factor in determining the threshold power. For droplets with radius comparable to the beam waist, $a \cong r_0$, in which all LC molecular dipoles in the droplets interact with a tightly focused laser beam and are directly reoriented by the light, the reconfiguration undergoes at the lowest threshold power. For larger droplets with $a > r_0$, the relevant scale for the interactions is limited in the small volume of focal spot. Thus, the LC molecules at the positions $r > r_0$ inside the droplet are reoriented either by the propagation of optical reorientation at the focal spot due to cooperative effects or by the small light field of transverse Gaussian intensity, leading to a higher threshold power for a larger droplet. This interpretation is clearly demonstrated by the tendency of the threshold power in the experiment (Figure 2.3). However, this finding contradicts essentially to the prediction of the OFT threshold by conventional light irradiations (Eqn. 2.1), by which the threshold is inversely proportional to square of droplet diameter. To clarify this issue, here, we evaluate the optical reorientation and reconfiguration by a tightly focused laser beam as follows.

Firstly, we consider the interaction energy of LCs aligned throughout the inside of the droplet by the electric field of the focused beam can be expressed as $U(r,z) \propto -\int \alpha Q I(r,z) dV$, where α is polarizability, I(*r*,*z*) is the light field intensity as a function of the lateral (*r*) and axial (*z*) distances from the center of the focal spot, V is volume of the droplet, and Q is dimensionless factor for the target materials in the geometrical optics regime [38]. In our realistic experiments, the light intensity distribution of an axial symmetric

Gaussian beam around the focus area is approximately expressed as, $I(r,z) = I_0 \exp\left(-2kr^2/(kr_0^2 + 4z^2)\right)$, where I_0 is the light power intensity at the center of focal spot is *k* wavenumber in the surrounding medium. Secondly, since the light-induced reconfiguration always competes with LC droplet-liquid interfacial anchoring effect [39], just like a system consisting of two-coexisting processes, namely, an optical controlled-lattice site surrounded by the interface-controlled self-aligned geometric configuration, we evaluate qualitatively the threshold of light-induced reconfiguration based on the mean-field theory [40]. In this case, we take into account the surface free energy of the droplet-liquid interfacial anchoring effect, which is defined as the multiplication of surface free energy per unit area (β) and the phase boundary area [26]. Considering that the depth of focus of the near-infrared laser beam is much smaller in the front of the droplet size, the total energy can be approximately given by,

$$U_{total} \propto -\frac{\alpha Q I_0}{\beta}\int_0^a r^2 \exp(-\frac{2r^2}{r_0^2})dr + a^2 \qquad (2.2)$$

This equation indicates that the total energy is a function of the radius of the droplet and laser power in terms of a and $\alpha QI_0/\beta$. We show in Figure 2.4(a) that the total energy shows a negative local minimum when $\alpha QI_0/\beta$ is larger than 7.5, indicating clearly that when the laser powers is above such a threshold condition, the interaction energy of the LCs realignment by the electric field overcomes the surface free energy of the droplet-liquid

interface, and thus, molecular reconfiguration can undergo throughout the inside of the droplet [29]. To place the droplet-size dependence in context, with the criterion that the total energy reaches a negative local minimum, in Figure 2.4(b) we show the polarization-insensitive plot of $\alpha Q I_0/\beta$ as a function of a/r_0, indicating two distinct regions in the plane of parameters; where in the region above the graph, the optical trapping is followed by molecular reconfiguration throughout the inside of the droplet. The slightly higher threshold power for the circular polarized beam can be understood as a cause of angular momentum transfer of the light inducing the rotation of the trapped droplet prior to the reconfiguration. From the plot, it now became clear that a larger threshold power is required for a larger droplet. The qualitative similarity between the tendency predicted by the calculation and that in the experimental observation supports the relevance of the above mentioned approximation.

Finally, for droplets with diameter much larger than the beam waist, in this case $a > 1$ μm, the predicted tendency shows a larger increase than that of the experimental observation. This fairly indicates that some parameters in Eqn. (2) may change drastically for the droplets with $a >> r_0$, resulting in such deviation from the experimental data. The physical reasons are yet unclear, though one may consider that Q is also a function of droplet-size [38]. The other likely reason for the deviation is that optical reorientation of LCs directly by the polarized focused beam is coupled with cooperative effects inside the droplet

through dipolar interaction, which may reduce the threshold power. We recall that such cooperative effects of smectic layers in the thin slab film results in a significant reduction of the predicted critical electric field at which the OFT effect takes place [41]. Hence, further investigations are still meaningful to find a possibility of obtaining a quantitative explanation.

(a)

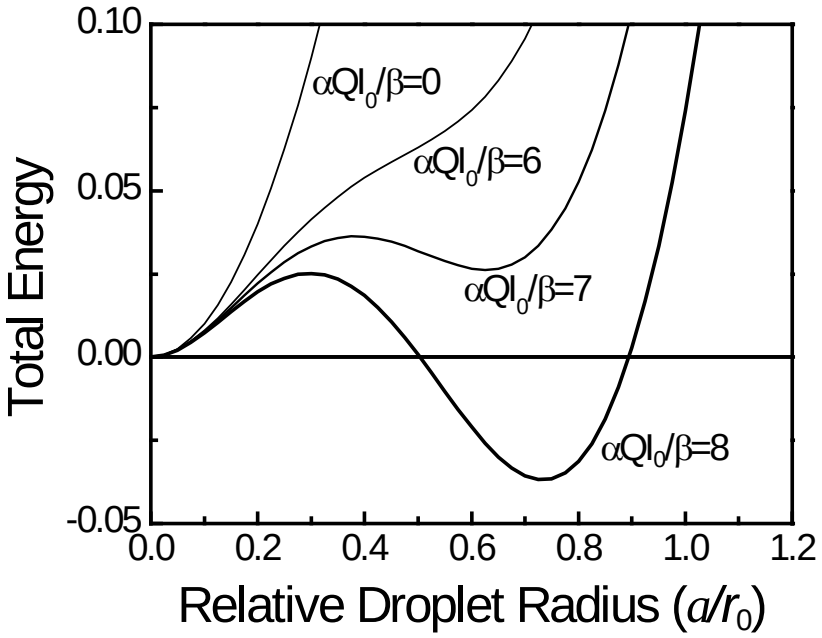

(b)

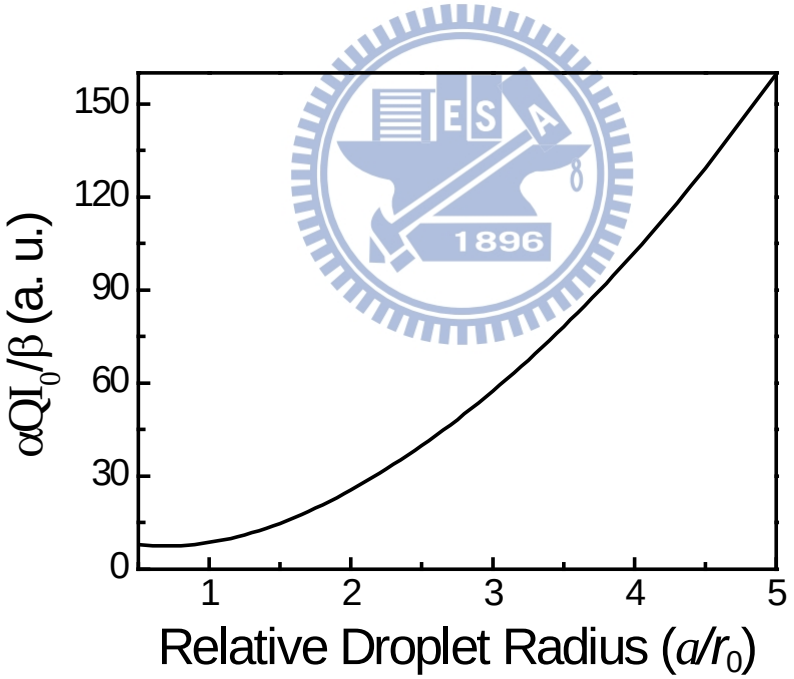

Figure 2.4 (a) The total energy as a function of the radius of the droplet at different level of laser power. (b) Plot of the predicted dependence of threshold laser power density to induce a negative local minimum, which is related to the reconfiguration, as a function of droplet radius relative to the beam waist, based on Eqn. (2.2) (see text for details).

5. Summary

We have presented laser-induced reconfiguration of micrometer-sized radial symmetric droplets of liquid crystal 5CB dispersed in D_2O. The definite threshold laser power to induce such reconfiguration depends on the droplet size and polarization state. The tendency of the droplet size dependence can be qualitatively explained by considering that the direct optical reorientation by laser beam is mostly distributed around the focal spot and that the LC droplet is a self-organized structure with droplet-liquid interfacial layer controlling the molecular orientation inside the droplet, rather than by conventional non-focused light irradiations. Thus, the likely mechanism involves the optical reorientation (OFT effect) at the focal volume and propagating out of the focal spot by cooperative effect. When the interaction energy of the LCs realignment by the electric field overcomes the surface free energy of the droplet-liquid interface, the radially symmetry of the radial symmetric structure is completely broken, and ultimately leading to a reconfiguration throughout the inside of the confined droplet. With this proposed mechanism, we show qualitatively that the calculated tendency of threshold power as a function of droplet size is in agreement with the experimental data.

6. References

[1] A. Ashkin, Phys. Rev. Lett. 24 (1970) 156.

[2] A. Ashkin, Proc. Natl. Acad. Sci. USA 94 (1997) 4853.

[3] A. Ashkin, J. M. Dziedzic, J. E. Bjorkholm, S. Chu, Opt. Lett. 11 (1986) 288.

[4] K. Sasaki, M. Koshioka, H. Misawa, N. Kitamura, H. Masuhara, Jpn. J. Appl. Phys. 30 (1991) L907.

[5] A. Ashkin, J. M. Dziedzic, T. Yamane, Nature 330 (1987) 769.

[6] P. Borowicz, J. Hotta, K. Sasaki, H. Masuhara, J. Phys. Chem. B 101 (1997) 5900.

[7] J. Hofkens, J. Hotta, K. Sasaki, H. Masuhara, T. Taniguchi, T. Miyashita, J. Am. Chem. Soc. 119 (1997) 2741.

[8] J. Hotta, K. Sasaki, H. Masuhara, J. Am. Chem. Soc. 118 (1996) 11968.

[9] Y. Tanaka, H. Yoshikawa, H. Masuhara, J. Phys. Chem. B 110 (2006) 17906.

[10] T. Sugiyama, T. Adachi, H. Masuhara, Chem. Lett. 36 (2007) 1480.

[11] Y. Tsuboi, T. Shoji, N. Kitamura, J. Phys. Chem. C 114 (2010) 5589.

[12] T. Sugiyama, T. Adachi, H. Masuhara, Chem. Lett. 38 (2009) 482.

[13] T. Rungsimanon, K. Yuyama, T. Sugiyama, H. Masuhara, N. Tohnai, M. Miyata, J. Phys. Chem. Lett. 1 (2010) 599.

[14] T. Rungsimanon, K. Yuyama, T. Sugiyama, H. Masuhara, Cryst. Growth Des. 10 (2010) 4686.

[15] T. Uwada, T.Sugiyama, H. Masuhara, J. Photochem. Photobiol. A: Chemistry 221 (2011) 187.

[16] X. Sun, B. A. Garetz, M. F. Moreira, P. Palffy-Muhoray, Phys. Rev. E 79 (2009) 021701.

[17] A. Usman, T. Uwada, H. Masuhara, J. Phys. Chem. C 115 (2011) 11906.

[18] S. Joudkazis, M. Shikata, T. Takahashi, S. Matsuo, H. Misawa, Appl. Phys. Lett. 74 (1999) 3627.

[19] S. Joudkazis, S. Matsuo, N. Murazawa, I. Hasegawa, H. Misawa, Appl. Phys. Lett. 82 (2003) 4657.

[20] T. A. Wood, H. F. Gleeson, M. R. Dickinson, A. J. Wright, Appl. Phys. Lett. 84 (2004) 4292.

[21] H. F. Gleeson, T. A. Wood, M. Dickinson, Phil. Trans. Royal Soc. A 364 (2006) 2789.

[22] Y. Yang, P. D. Brimicombe, N. W. Roberts, M. R. Dickinson, M. Osipov, H. F. Gleeson, Opt. Express 16 (2008) 6877.

[23] E. Brasselet, N. Murazawa, S. Joudkazis, H. Misawa, Phys. Rev. E 77 (2008) 041704.

[24] E. Brasselet, S. J. Joudkazis, Nonlinear Opt. Phys. Mater. 18 (2009) 167.

[25] N. Murazawa, S. Joudkazis, H. Misawa, Eur. Phys. J. E 20 (2006) 435.

[26] P. G. de Gennes, J. Prost, The Physics of Liquid Crystals, 2nd ed.; Clarendon Press: Oxford, 1993.

[27] A. I. Bishop, T. A. Nieminen, N. R.; Heckenberg, Rubinsztein-Dunlop, H. Phys. Rev. Lett. 92 (2004) 198104.
[28] N. Murazawa, S. Joudkazis, V. Jarutis, Y. Tanamura, H. Misawa, Eur. Phys. Lett. 2006, 73, 800.
[29] A; Usman, W.-Y; Chiang, T; Uwada, H. Masuhara, Proc. SPIE 8274 (2012) 82740L1-8.
[30] S. Joudkazis, N. Mukai, R. Wakaki, A. Yamaguchi, S. Matsuo, H. Misawa, Nature 408 (2000) 178.
[31]S. Ito, T. Sugiyama, N. Toitani, G. Katayama, H. Miyasaka, J. Phys. Chem. B, 111 (2007) 2365-2371.
[32] N. Murazawa, S. Joudkazis, S. Matsuo, H. Misawa, Small 1 (2005) 656.
[33] N. Murazawa, S. Joudkazis, H. Misawa, Opt. Express 14 (2006) 2481.
[34] P. Palffy-Muhoray, The Nonlinear Optical Response of Liquid Crystals. In Liquid Crystals: Applications and Uses; Bahadur B., Ed., World Scientific, New Jersey, 1990.
[35] I.-C. Khoo, S. T. Wu, Optics and Nonlinear Optics of Liquid Crystals; World Scientific: Singapore, 1993.
[36] I.-C. Khoo, R. R. Michael, P. Y. Yan, IEEE J. Quantum Electron QE-23 (1987) 267.
[37] E. Santamato, Y. R. Shen, Opt. Lett. 9 (1984) 564.
[38] A. Ashkin, Biophys. J. 61 (1992) 569.
[39] I. I. Smalyukh, S. Chernyshuk, B. I. Lev, A. B. Nych, U. Ognysta, V. G. Nazarenko, O. D. Lavrentovich, Phys. Rev. Lett. 93 (2004) 117801.
[40] S. A. Safran, Statistical Thermodynamics of Surfaces, Interfaces, and Membranes, Westview: Colorado, USA, 2003 (2003).
[41] X. Y. Wang, T. Kyu, A. M. Rudin, P. L. Taylor, Phys. Rev. E 58 (1998) 5919

CHAPTER 3

Optical Trapping and Polarization-Controlled Scattering of Dielectric Spherical Nanoparticles by Femtosecond Laser Pulses

1. Introduction

One of the successful applications of mode-locked lasers is the ultrafast time-resolved spectroscopies, which provide the absorption, vibrational, or emission spectra of atoms or molecules on extremely short time scales after their excitation with ultrashort laser pulses. The research group of Prof. M. Martin is one of pioneers who have utilized transient absorption spectroscopy to decipher the dynamics and mechanisms of fundamental photo-induced processes [1]. Their reports on the insights of driving forces and primary occurring events in the photo-induced dynamics of various chromophores, photoactive proteins, or biomimetics are important advances in our understanding of the photo-processes, particularly the functionality of the biomaterials in relation with their electronic structures [2–7].

Another important laser application is optical trapping (also called optical tweezers), exploiting the optical gradient force, which can confine micrometer to a few tens nm-sized objects in the focal spot [8,9]. In this phenomenon, a high numerical aperture lens is necessarily required to focus tightly the continuous-wave (cw) laser beams into a diffraction-limited spot size [10,11]. With its potential ability of non-destructive tool to immobilize, reorient, and transfer the dielectric or metallic particles, this technique has been widely applied in various fields of sciences with target materials ranging from small particles [12], polymers [13,14], clusters of amino acids [15–19], to biological substances [20], and has

become indispensable in single-molecule measurements [21,22].

Recently, the optical trapping technique is further developed by utilizing ultrashort laser pulses. By the femtosecond laser pulses, optical trapping of micrometer-sized silica spheres was found to be as just effective as cw optical tweezers, and trap stiffness was related to average power of the laser pulses [23]. With the ultrashort laser pulses, however, several phenomena have been revealed, including optical trapping of as small as a few nm-sized CdTe quantum dots or the depositions of CdS nanoparticles with grain size down to 25 nm [24,25]. For the trapping of gold nanoparticles by laser pulses, the trapping site splits up into two equivalent positions around the focal center, demonstrating that high nonlinear optical susceptibility of the target materials can modify the shapes of gradient force and trapping potential [26]. More recently, the femtosecond laser pulses with the power less than 200 mW has been successfully applied to confine an individual polystyrene bead with a diameter of a few tens of microns (the particle sizes within the framework of geometrical optics regime), but the microparticle was pushed away from the trapping site when the focal position was shifted to its downstream surface due to secondary convergence of the laser pulses that reduces water breakdown threshold [27].

In this article, we report on an experimental study exploring the trapping behavior of the dielectric spherical nanoparticles (50-nm-diameter polystyrene beads), suspended in liquid water medium, by femtosecond laser pulses tightly focused by high numerical aperture

lens. We show that as compared with the cw mode, the laser pulses can trap a larger number of nanoparticles. In addition, the laser pulses induce nanoparticle flows out of the focal spot in two opposite directions, in an alternating manner, controlled by the laser polarization. To understand this phenomenon, we evaluate both radiation (gradient and scattering) and temporal forces (the latter is also called pulse radiation force) by adopting Lorentz force of fundamental Gaussian beam exerted on Rayleigh particles [10,28], and by applying scattering cross section value of the nanoparticles obtained based on Mie theory [29]. We demonstrate that the axial electric field produced by the high numerical aperture objective lens is responsible for the present novel phenomenon.

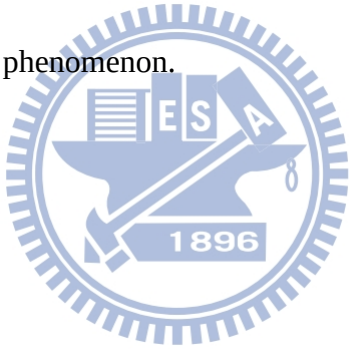

2. Experimental

2.1 Optical setup

To experimentally exemplify the trapping behavior of the nanoparticles by femtosecond laser pulses, we developed an experimental setup based on an inverted microscope (Olympus IX71), as shown in upper Figure 3.1. We used a 800-nm fundamental mode of Ti:sapphire (Tsunami; Spectra Physics) laser beam, which can be operated in cw or femtosecond-pulse mode, acting as the trapping beam. When it was operated in the pulse mode, the pulse duration was compressed by a pair of prisms to be about 90 fs, and the repetition rate was 80 MHz. The polarization direction of the laser beam was controlled by a half-wave plate before the beam was collimated and expanded to ~5 mm in diameter by a pair of positive lenses with focal length being 100 and 200 mm, respectively. The beam then was focused through an objective lens (60×, NA = 0.90) at normal incidence into a sample cell, which was placed on the sample stage of the microscope. The light power after the objective lens was controlled in the range of 0.10–0.35 W. The beam waist, ω_0, at the focal spot was calculated to be 460 nm, equivalent to the calculated radius when the beam intensity of its first Airy pattern falls to $1/e^2$ of the maximum value.

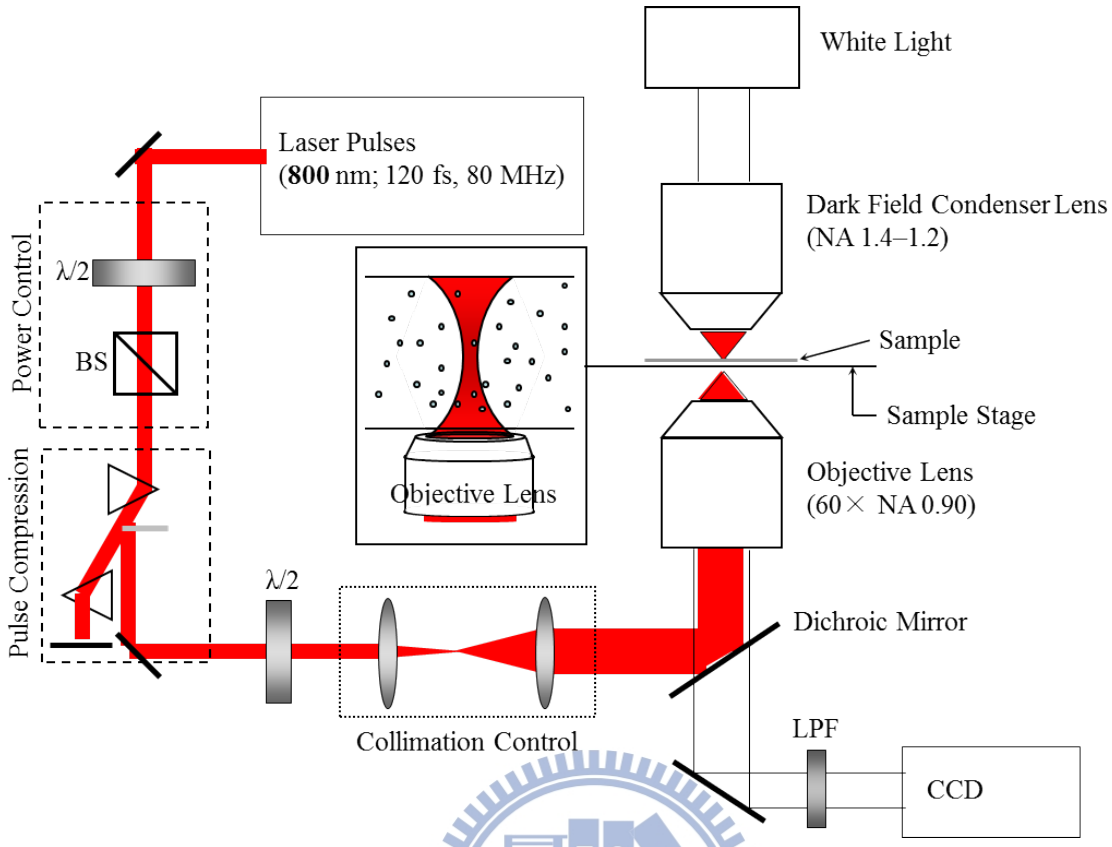

Figure 3.1 Schematic diagram of the experimental set-up; λ/2 is halfwave plate, BS is beam splitter, and LPF is low pass filter. Inset is a schematic illustration of the sample cell containing the colloidal solution of nanoparticles.

2.2 Sample cell and detection system

The sample cell consisted of a silicon chamber (1 mm thickness) sandwiched between two cover-glass plates (Matsunami). The inner well of the chamber (10 mm in diameter) was filled with colloidal solution containing spherical polystyrene beads (PolyScience; radius = 25 nm, density = 1.06 g/cm^3) suspended in distilled water (refractive index = 1.33 at room temperature). Concentration of the polystyrene beads was 3.79 × 10^{14} particles/mL. The refractive index of the polystyrene nanoparticles at 800 nm wavelength was

calculated by Cauchy dispersion relation to be 1.59 [30].

The sample cell containing the dielectric spherical nanoparticles was illuminated by white light (λ = 400–750 nm) from a halogen lamp passing through a cardioid immersion dark field condenser lens (Olympus; U-DCW NA = 1.4–1.2). The elastic light scattering originated from the laser trapping beam was completely cut by a shortwave-pass filter with transmission at 380–720 nm (Semrock; Brightline 750/SP) in front of charge-coupled device (CCD) camera (JAI; CV-A551R E). With such a setup only the scattering light from halogen lamp by the nanoparticles was collected by the objective lens, and was detected by using the CCD camera running at 30 interlaced frames per second. Thus, the detected light intensity can be related mainly to the scattering light intensity, although there is possibly a very minor contribution of three-photon excited fluorescence of the bare polystyrene beads due to nonlinear optical effects if such the fluorescence wavelength is longer than 380 nm to pass the shortwave-pass filter. The positions of the nanoparticles were associated with the image of the scattering light detected by the CCD camera. The resolution of the image in the lateral direction was 94 nm per pixel, and our observation layer was limited within the axial resolution of the objective lens (calculated to be approximately 1.8 μm).

3. Results

3.1 Polarization-controlled off-axis scattering of nanoparticles

With the laser trapping beam operated in the femtosecond pulse mode at the average power of 350 mW, we observed a brighter scattering light at the focal spot compared with the surrounding area. We should note that such bright scattering light was never observed in a neat solvent. In addition to scattering light at the focal spot, bright locus of scattered polymer beads, just like multiple shooting stars, from the focus spot to the surrounding area was also observed. The bright locus was shaped like a partially opened folding fan along two opposite directions, in an alternating manner, perpendicular to the polarization direction. Such the event occurred randomly, and simultaneous bright locus along the two opposite directions like a pair of two partially opened folding fans was never observed. Thus, we show the bright locus along the two opposite directions by combining two halves of different video frames in Figure 3.2(a)–(c). Since the scattering lights detected in the video image represent the positions of the nanoparticles, we therefore extracted the profiles of scattering light intensity passing through the focal center as shown in each panel. Such line profile parallel to the polarization direction shows clearly a single sharp peak with an approximately 1.6 μm full width at half maximum at the focal spot, whereas that perpendicular to the polarization direction indicates the additional bright locus of scattered polymer beads along the two

opposite directions in an alternating manner. The intensity of the bright locus is comparable to each other. When the laser beam was operated in the cw mode at the same laser power, only a tiny scattering light at the focal spot was observed under the similar experimental conditions, but there were no any observable bright locus of scattered polymer beads from the beam center to the surrounding area. An image frame under the cw-mode laser irradiation is shown in Figure 3.2(d). The line profiles passing through the focal center parallel and perpendicular to the polarization direction reveal that the scattering light at the laser focal spot of the cw mode is very low.

By varying the laser power, the threshold of the femtosecond laser pulses to induce observable scattering light at the focal point and bright locus along the two opposite directions was observed at 264 mW for the highly concentrated nanoparticle solution. We also found that the concentration of the nanoparticles was a crucial parameter to observe the bright locus. Under the same optical conditions, the laser pulses at the average power of 350 mW, the bright locus was not observed when the solution was diluted by a factor of 4, equivalent to the concentration of 0.95×10^{14} particles/mL. The fourfold dilution led to severe reductions in the trapping rate, size of trapped assembly, and number of scattered nanoparticles, giving no bright locus.

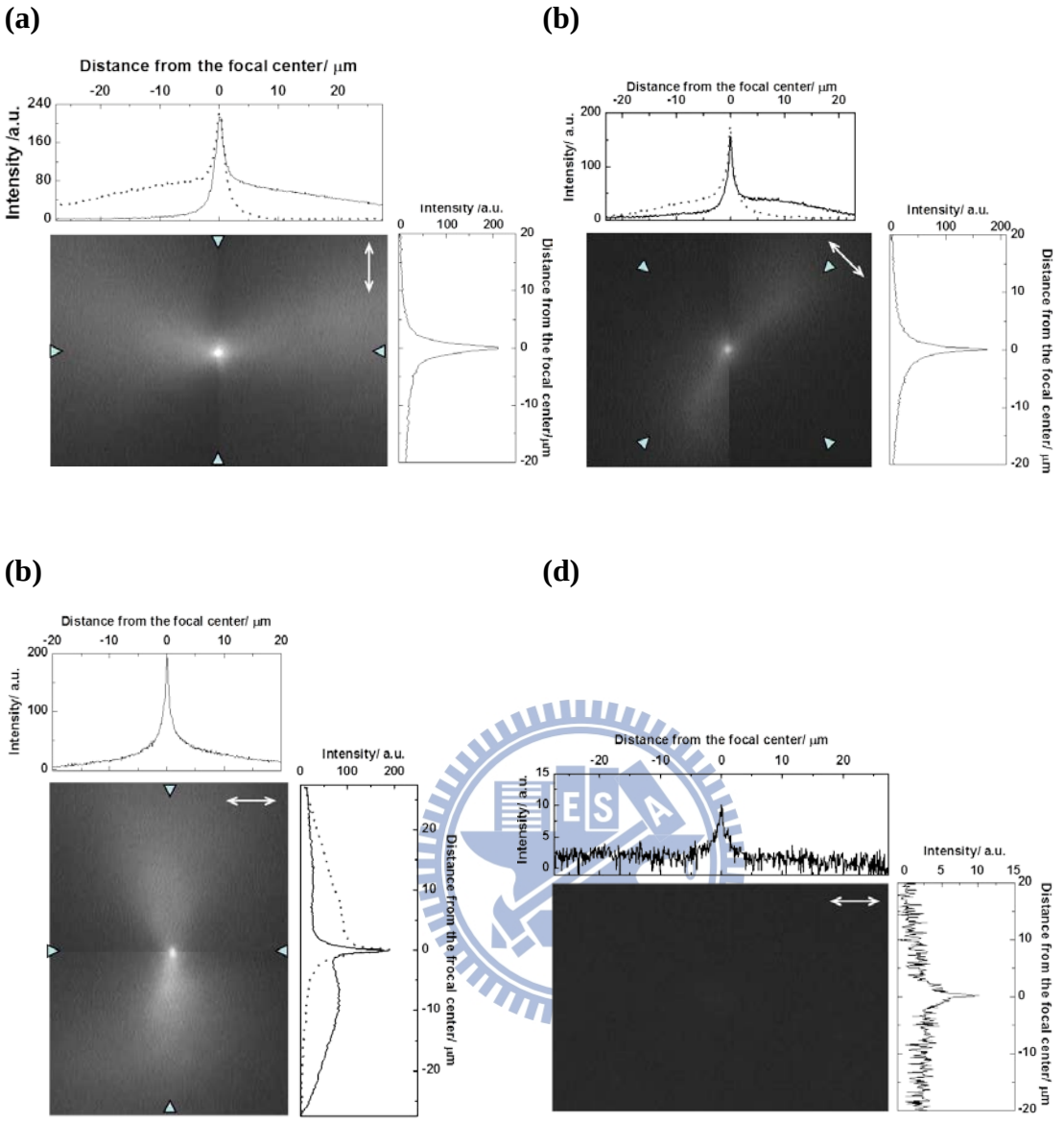

Figure 3.2 A combination of two halves of two different image frames showing optical trapping and scattered polystyrene nanoparticles by femtosecond-pulse modes and showing their optical trapping by cw Ti:sapphire laser beams (λ= 800 nm). (a)-(c) A sharp scattering light at the focal spot and bright locus of scattered polymer beads from the focus spot to the surrounding area towards two opposite directions in an alternating manner perpendicular to the laser polarization direction of femtosecond laser pulses, indicating the optical trapping of polystyrene nanoparticles at the focal spot and nanoparticle flows along the two opposite directions. The laser power for each case is 350 mW after the objective lens. Arrow in each panel indicates polarization direction of the laser beam. The line profiles in each panel were taken from one cursor passing through the focal center to the opposite cursor, parallel and perpendicular to the polarization direction. The two line profiles (solid and dotted lines) perpendicular to the polarization direction are related to the two alternating directions of the scattering light. (d) An unstable and low scattering light intensity from the focal spot of cw laser beam at the same laser power. Arrow in the panel indicates polarization direction, and the line profiles were taken from parallel and perpendicular to the polarization direction.

3.2 Temporal evolutions of the bright spot at the focal spot

The temporal evolutions of scattering light intensity at the focal spot when the laser beam was operated in femtosecond-pulse or cw mode are shown in Figure 3.3(a). In contrast to high intensity of scattering light when the laser beam was operated in the pulse mode, low intensity, unstable, and fluctuated scattering light intensity was observed under the cw mode. In comparison, the scattering light intensity is about one order higher when the laser beam was operated in the pulse mode than that under cw mode.

Further, in Figure 3.3(b) we show the plot of the temporal random distribution of the event, where the bright locus was observed along one of the two alternating directions perpendicular to the polarization of the femtosecond laser pulses, for the observation window about 120 s. The bright locus emerged in one direction on the timescale of seconds before they changed into the opposite direction, and they continued in the same way. The probability and total duration of the bright locus along the two alternating directions almost balanced each other.

(a)

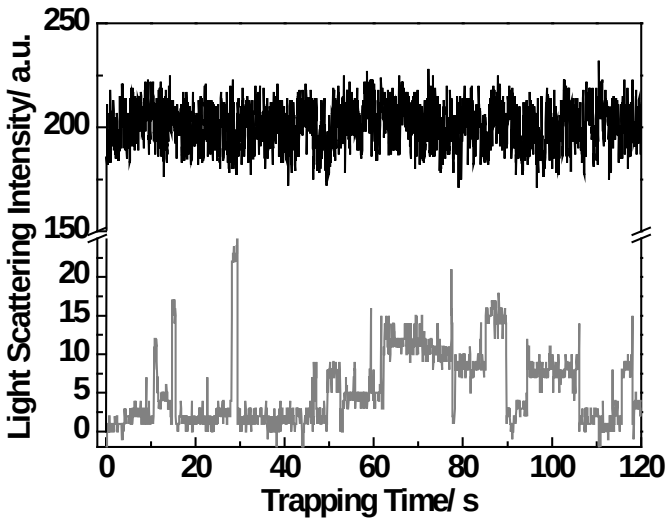

(b)

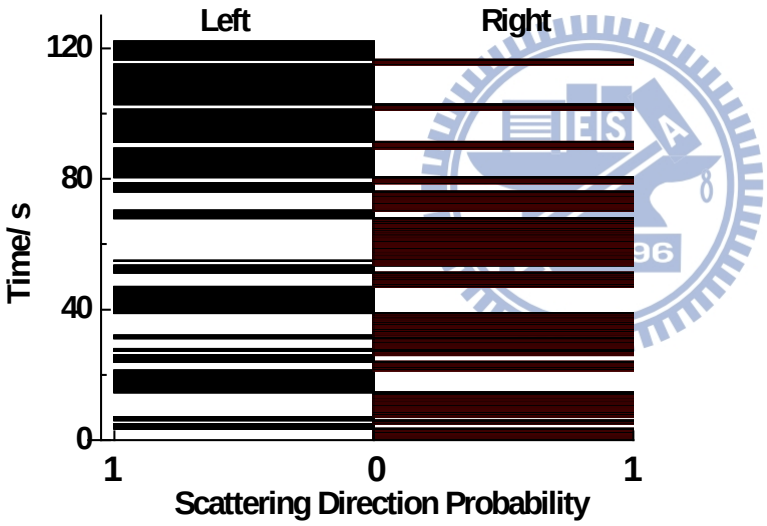

Figure 3.3 (a) Time-dependent line profile intensity under femtosecond-pulse (black line) and cw mode (gray line). (b) The typical time-dependent event when bright locus of scattered polymer beads from the focus spot is along the two alternating left and right directions within the observation window of 120 s. Experimental information for data shown in the figures (a) and (b) are related to those in Figure 3.2a.

4. Discussion

4.1 Optical trapping and nanoparticle flows

Extracting the intensity of scattering light by line profile is one of useful practical ways to identify the spatial position of nanoparticles in colloidal solution. Typically, a sharp light intensity at the focal spot in the line profiles can be attributed to nanoparticles accumulated by laser trapping, and the number of trapped nanoparticles is associated with the light intensity [31]. Similarly, the existence of such single and sharp peak intensity from the spherical polystyrene beads under the femtosecond laser pulses, as shown in Figure 3.2, indicates the possible of a single trap site at the focal spot. Such a single trap site is commonly observed in conventional optical trapping experiments [8] and [32], but it is in contrast to the trap split of 60-nm sized gold nanoparticles by the femtosecond laser pulses on the same level of average laser power [26]. It is noteworthy that since the third-order nonlinear optical susceptibility is responsible and sensitive to split the trap site into two equivalent positions shifted from the beam axis, the lower third-order susceptibility of polystyrene nanoparticles (0.8×10^{-8} esu) [33] as compared with that of gold nanoparticles (5×10^{-8} esu) [34] is the reason for the polymer nanoparticles having no clear observable nonlinear optical effect on the trap site.

Here, we interpret our experimental results as follows. When a nanoparticle enters the effective trapping area by diffusion, gradient force due to a steep gradient of optical

intensity of the highly focused ultrashort laser pulses is exerted on the nanoparticle, and the force drags the nanoparticle towards the single trap site at the focal center. A stable trapping can only be achieved when the gradient force overcomes scattering force, and the characteristic stiffness of optical trap should be proportional to the laser intensity, as it has been reported for the trapping laser in cw mode [21] and [35]. For the ultrashort optical pulses, in particular, in addition to the gradient and scattering forces, we also have to consider temporal force within the pulse duration, which is defined as instantaneous Lorentz force at the time over the entire duration of the pulse envelope [36], [37] and [38]. In this case, the gradient force of the laser pulses should overcomes the scattering and their temporal forces to achieve a stable trapping. Considering the sizes of the nanoparticles and beam waist, multiple nanoparticles can be trapped in the single potential minimum at the focal spot, and the scattering light intensity is proportionally enhanced with the number of trapped nanoparticles at the trap site. Thus, monitoring such the scattering light intensity, similarly to monitoring a stepwise behavior of fluorescence intensity increase in optical trapping of 100- or 200-nm-sized dye-doped polystyrene nanoparticles by cw laser beam [39], would provide the information on the number of nanoparticles entering the trap site. However, the video frames in our experiment are saturated within the first integrating time, hindering a precise observation on the exact number of the optically trapped nanoparticles. Nevertheless, based on the scattering light intensity at the focal spot (Figure 3.3(a)) we could roughly estimate the

number of trapped nanoparticles to be at least one order higher when the laser is operated in the femtosecond pulse mode compared with that under cw mode on the same averaged laser power.

Since the optical trapping potential can only filled by a certain number of nanoparticles, additional nanoparticles entering the trapping site should push and replace the nanoparticles occupying the trapping site. The trapped nanoparticles can also escape and release themselves from the trapping site by diffusion during the interval period between two laser pulses. The nanoparticles escaped from the optical trapping site are readily pushed farther away from the focal center by scattering or temporal forces. Although one single pulse may not be able induce the migration of nanoparticles along the way as they are observed in this present work, but since the laser pulses are repeatedly introduced at the pulse repetition rate of 80 MHz into the highly concentrated nanoparticles, we consider that multiple nanoparticles are scattered with the high frequency on the same direction. With this mechanism, the stable quantity of nanoparticles at the trapping site is maintained, resulting in the constant intensity of line profiles observed at the trapping site, while multiple nanoparticles are continuously scattered out of the focal spot making their motions as a kind of nanoparticle flow, which is observed as the multiple shooting stars from the focal spot to the surrounding area forming a partially opened folding fan-shaped bright locus. Interestingly, the nanoparticle flows are along two opposite directions, in an alternating manner, controlled

by the laser polarization. In the following, we show that such the polarization-controlled nanoparticle flows can be attributed to the existence of lateral component of scattering and temporal forces.

4.2 Radiation and temporal forces acting on a dielectric spherical nanoparticle

Let us consider the fundamental mode of Gaussian beam propagating without distortion in a medium containing dielectric spheres. The beam is tightly focused by a high numerical aperture objective lens, converging to a near-diffraction-limited size with a focal waist being ω0, and then reexpanding. Here, we consider that Lorentz force acts on a dielectric spherical nanoparticle due to interactions between light electric field and induced dipole moment of the polarizable dielectric sphere. The induced polarization can be approximately expressed as, P = χE, where χ is the electric susceptibility. For a uniform dielectric sphere, the susceptibility is isotropic and the polarization P is parallel to E. Thus, the gradient force, related to spatial Lorentz force, exerted on the nanoparticles can be expressed as [28]

$$\mathbf{F}_{\text{grad}} = [\mathbf{P}\cdot\vec{\nabla}]\mathbf{E} = \frac{1}{2}\alpha\vec{\nabla}\left|\mathrm{E}\right|^2 \qquad (3.1)$$

where $\alpha = 4\pi \mathrm{n}_{\mathrm{m}}^2 \varepsilon_0 a^3[(m^2-1)/(m^2+2)]$ is the polarizability of an individual nanoparticle in the Rayleigh regime, ε_0 is vacuum permittivity, a is the radius of the nanoparticle,

and m=np/nm is the relative refractive index of the particle (n_p) to medium (n_m). Another component in the radiation force is the scattering force due to momentum transfer of light exerting on the dielectric sphere, as given by

$$\mathbf{F}_{scatt} = (n_m \sigma_p / c)\langle \mathbf{E} \times \mathbf{H} \rangle_t \qquad (3.2)$$

where σp is the scattering cross section of a nanoparticle, c denotes the speed of light in vacuum, and $\langle \mathbf{E} \times \mathbf{H} \rangle_t$ is the time-averaged energy flux of the laser pulses. The temporal force is given by [36], [37] and [38]

$$\mathbf{F}_{temp} = \mu_0 \partial_t \langle \mathbf{P} \times \mathbf{H} \rangle = \alpha \mu_0 \partial_t \langle \mathbf{E} \times \mathbf{H} \rangle \qquad (3.3)$$

where μ_0 is vacuum permeability. The character and magnitude of this temporal force depend strongly on the pulse duration [40], and this force is obviously zero for the cw laser beams.

It is noteworthy that in our experimental case, for wavelength of laser beam λ = 800 nm and beam waist ω_0 = 460 nm, beam divergence half-angle (defined as $\theta = \lambda/\pi n_m \omega_0$) is calculated to be ~24°. Consequently, the axial vector field of the plane-polarized Gaussian beams tightly focused by such an objective lens can not be neglected [41] and [42]. If we assume the focal plane is located at the xy-plane (z = 0), and the carrier frequency and pulse duration of the laser pulses is ω and τ, respectively, the linearly polarized electric field parallel to the x-axis can be expressed as $E_{x0} = E_0 \exp[i\omega t - \xi^2]\exp[-\tilde{t}^2]$ (where $\xi = x/\omega_0$ and $\tilde{t} = t/\tau$). We note that the electric field along the y-axis is zero in the lowest order approximation of the paraxial Gaussian beam [41] and [43], and the axial electric field along the z-axis can be derived using

$E_{z0}=(-i/k)\partial_x E_{x0}$, and one obtains

$$E_{z0} = -iK\xi\, E_0 \exp[i\omega t - \xi^2]\exp[-\tilde{t}^2] \tag{3.4}$$

where $k=2\pi/\lambda$ and $K=2/k\omega_0$. By considering that the axial component is a phase quadrature, the electric field on the *x*-axis is given by [26], $\mathbf{E} = E_0(\hat{x}\cos\omega t + \hat{z}K\xi\sin\omega t)\exp[-\xi^2]\exp[-\tilde{t}^2]$ (where $\hat{x}$ is the unit vector along the *x*-axis, and $\hat{z}$ is the unit vector of *z*-axis or along the beam propagating direction). With the corresponding magnetic field of the laser pulses, $\mathbf{H} = n_m\varepsilon_0 c(\hat{x}E_{z0} + \hat{y}E_{x0})$ the gradient, scattering, and temporal forces exerting on a nanoparticle at the focal plane, as presented in Eqs. (3.1), (3.2) and (3.3), can be therefore expressed as follows

$$\mathbf{F}_{grad} = -\hat{x}\,\alpha E_{x0}^2[\xi/\omega_0 - \tfrac{1}{2}K^2\xi/\omega_0 + K^2\xi^3/\omega_0] \tag{3.5}$$

$$\mathbf{F}_{scatt} = \hat{z}(n_m^2\sigma_p\varepsilon_0/2)E_{x0}^2 + \hat{y}(K^2\xi^2 n_m^2\sigma_p\varepsilon_0/2)E_{x0}^2 \tag{3.6}$$

$$\mathbf{F}_{temp} = -\hat{z}\,4\alpha\, n_m E_{x0}^2\,\tilde{t}/c\tau - \hat{y}\,4\alpha\, n_m E_{x0}^2 K^2\xi^2\,\tilde{t}/c\tau \tag{3.7}$$

We note that the gradient force has only a lateral component, whereas the scattering and temporal forces have two orthogonal components perpendicular to the electric field E_{x0} direction; along the beam propagation direction and in the lateral y-axis. The magnitudes of the gradient, scattering, and temporal forces depend on the laser beam intensity and on the spatial position in the trapping area, and in particular, the temporal force is also inversely proportional to pulse duration. The effect of the axial component field produced by the high-numerical aperture objective lens arises clearly in the gradient, scattering, and temporal

forces in the term K^2. It is therefore interesting to calculate the forces in our real experimental case.

From knowledge of the size and refractive index of an individual polystyrene nanoparticle we calculated ˛ to be 3.85×10^{-34} N m^3V^{-2}, and based on the Mie scattering theory [29] we obtained σ_p to be $3.5\times10^{-19}m^2$. By adopting the values of $K \approx 1.6/\pi$ for an objective lens with NA ≈ 0.9 [26,43] and $E_0 = (4P/\pi\omega_0^2 n_m \varepsilon_0 c)^{1/2} = 24.4$ V/μm, (where P = 350 mW is the average power of the femtosecond laser, corresponding to laser power intensity of 1.05×10^{12} W/m^2 at the focal center), in Figure 3.4(a) and (b) we show the plots of the calculated time-averaged gradient and scattering forces exerting on a spherical polystyrene nanoparticle as a function of the position x/ω_0. The lateral gradient force with the maximum being 0.14 pN at $x = 0.56\omega_0$ (shown in Figure 3.4(a)) acts as a restoring force, which directs the nanoparticle towards the beam center as commonly observed in conventional optical trapping experiments [8,32]. The maximum value of axial scattering force is 1.6 fN at x = 0, and that of lateral scattering force is 0.08 fN at $x = 0.71\omega_0$, as shown in Figure 3.4(b). Such the gradient and scattering forces of the time-averaged power of the mode-locked laser beam should also be applied for the cw laser beam. The calculated axial and lateral temporal forces, which apply only for the laser pulses, as a function of the time t/τ is plotted in Figure 3.4(c). The plot reveals that the temporal forces fluctuate within the pulse envelope (τ= 90 fs), similarly to the theoretical approach reported by Gordon [36] and Wang and Chai [40]. At the

first half of the pulse, the axial and lateral component of the temporal force pushes the nanoparticles along the beam propagation and along y-axis, respectively, parallel to those of the scattering force. At the second half of the pulse the temporal force pushes the nanoparticles along the opposite directions. Interestingly, the maximum axial and lateral temporal forces were estimated to 12.3 fN and 1.7 fN, respectively, which are about 8 and 20 times larger than the respective component of scattering force. Those gradient, scattering, and temporal forces are illustrated with a diagrammatic sketch in Figure 3.4(d).

Considering that the optical trapping relies on the lateral gradient force, and that the magnitude of the lateral gradient force at the focal plane overcomes those of the scattering and temporal forces, the optical trapping of 50-nm diameter polystyrene spheres by the ultrashort laser pulses is realized. Such optical trapping of the nanoparticles is also supported by the estimated potential energy to be 13.8 k_BT (at 300 K) at the beam center, which is above the minimum criterion of a necessary potential energy to overcome thermal energetic for a stable optical trapping (10 k_BT)[8,28]. When the polymer nanoparticles escape from the optical trapping potential, they are readily scattered out of the focal spot by the resultant of axial and lateral components of both scattering and temporal forces. In particular, the lateral scattering and temporal forces, which are much larger in the front of the gravity of the nanoparticle (6.9×10^{-4} fN), should control the nanoparticle flows in the directions perpendicular to the light field polarization.

4.3 Comparison between radiation forces on the nanoparticles in femtosecond laser pulses and in CW laser

If the necessary potential energy of pulsed laser beams to trap the nanoparticles is related to their average power, similarly to the case of cw laser beams, we estimated that, under our experimental condition, the axial optical trapping can be achieved at minimum laser power of 250 mW. This is in agreement with our observation (264 mW). However, the optical trapping behavior of the nanoparticles by laser pulses dramatically differs from that by cw laser beam in terms of the number of trapped nanoparticles and the existence of scattered nanoparticles towards the directions controlled by the laser polarization. The higher number of nanoparticles trapped at the focal spot (Figure 3.3(a)) by the laser pulses in comparison with that by cw mode indicates the higher optical trapping efficiency of the laser pulses, although the fluctuation of scattering light intensity at the focal spot takes place due to the dynamic particle motions during the pulse irradiation and pulse interval period. To clarify this issue, we consider the number of photons of the 800-nm laser beam transferred into the sample. For the laser pulses with an average power of 350 mW, the peak power of a single pulse is 4.9 nJ and the number of photons per second is 1.11×10^{23}, almost five orders higher than that of cw mode (1.41×10^{18}) for the same laser power, highlighting the impulsive peak power of the laser pulses in the front of cw mode. However, we should note that such a peak power in our experiment is much smaller than that to induce optical breakdown in water,

which requires 0.1 μJ per pulse for 100 fs laser pulses [44], generating shockwave emission and cavitation bubble [44–47]. Unlike the polystyrene particles containing fluorescent dyes [38], the bare polymer nanoparticles in our experiments does not absorb efficiently two-photon excitation of the laser pulses, thus, they are not ablated by the laser pulses. We should also note that the polystyrene nanoparticle size is too much smaller than the beam waist to induce secondary convergence of the femtosecond laser pulses that can reduce the optical breakdown threshold as observed for polystyrene beads with a few tens of micron in diameter [27]. Thus, under our experimental condition we can rule out the possible contributions of shockwave, cavitation bubble (related to optical breakdown), or ablation, in the mechanism of the nanoparticle flows controlled by the laser polarization. Instead, as we proposed in Section 4.2, the lateral components of both scattering and temporal forces during the short pulse irradiation play an important role in the polarization-controlled nanoparticle flows. The temporal force, which is not available in cw mode, pushes the nanoparticles in the fluctuating manner out of the focal center, inducing the dynamics of nanoparticle motion during the pulse duration. The particle motions may also induce convection of the liquid medium. Thus, combination of attractive and repulsive forces by the impulsive peak power, resulting in dynamic motions and diffusions of nanoparticles around the focal spot, makes optical trapping of laser pulses is more efficient than that of cw mode. In other words, under cw mode, the laser beam without modulation results in flat power, less controllable flows, less

dynamic motions and diffusions of nanoparticles around the focal spot, and hence, less efficiency in optical trapping.

In order to evaluate whether a trapped nanoparticle can escape from the trap site by thermal motion during the pulse interval period between two pulses, we have considered the diffusion of a polystyrene nanoparticle in water. With 12.5 ns interval between two laser pulses (related to 80 MHz repetition rate) and diffusion coefficient in the order of ~10^{-10} m^2 s^{-1} for 57-nm diameter polystyrene particle [48], we estimated the diffusion of the nanoparticles within the pulse interval period to be ~4 nm^2, which is much smaller than the focal spot size. We therefore could exclude the severe destabilization of the optical trapping due to the nanoparticle diffusion. Nevertheless, the diffusion during the interval between pulses may be attributed to the fluctuation of accumulated nanoparticles at the focal spot as indicated by the light intensity fluctuation in Figure 3.3(a). Since the existence of nanoparticle aggregate at the focal spot can distort the light electric field, we proposed that a certain macroscopic shape of the accumulated nanoparticles allows the nanoparticle flows in one direction and the other shape in another direction. In this current experimental case, such a transition from one to another macroscopic shape of the accumulated nanoparticles takes place on the time-scale of seconds, not on the time-scale of the pulse duration. This also indicates that the change or destabilization of macroscopic shape of the accumulated nanoparticles is much slower than the fluctuation in the number of the optically trapped

nanoparticles.

Further, we interpret that pulse duration and repetition rate of laser pulses will be important parameters governing and bringing about the efficient optical trapping and polarization-controlled scattering of the dielectric spherical nanoparticles. This interpretation is in contrast to the optical trapping of 0.78 or 1.28 μm silica spheres, in which the optical trapping of the submicro- or microparticles by femtosecond laser pulses were reported to be just as effective as those by cw laser mode, and the optical trapping is independent on pulse duration within 12–40 fs over the repetition rate of 80 MHz [23,38]. This can be understood as we have interpreted our results based on instantaneous force on the 50-nm sized Rayleigh particles instead of total impulse transfer by the laser over the repetition cycle on such micron-sized particles, which are much larger than the beam waist implemented in those reports [23,38]. Finally, experiments with varying repetition rate and pulse duration of laser pulses, in addition to anisotropy, the concentration of the colloid, and the intrinsic polarizabilities of the Rayleigh colloidal particles as extensions of our current study are in progress in our laboratory, pursuing generality of the trapping and polarization-controlled scattering of dielectric nanoparticles by the tightly focused laser pulses, and the results will be reported elsewhere in near future.

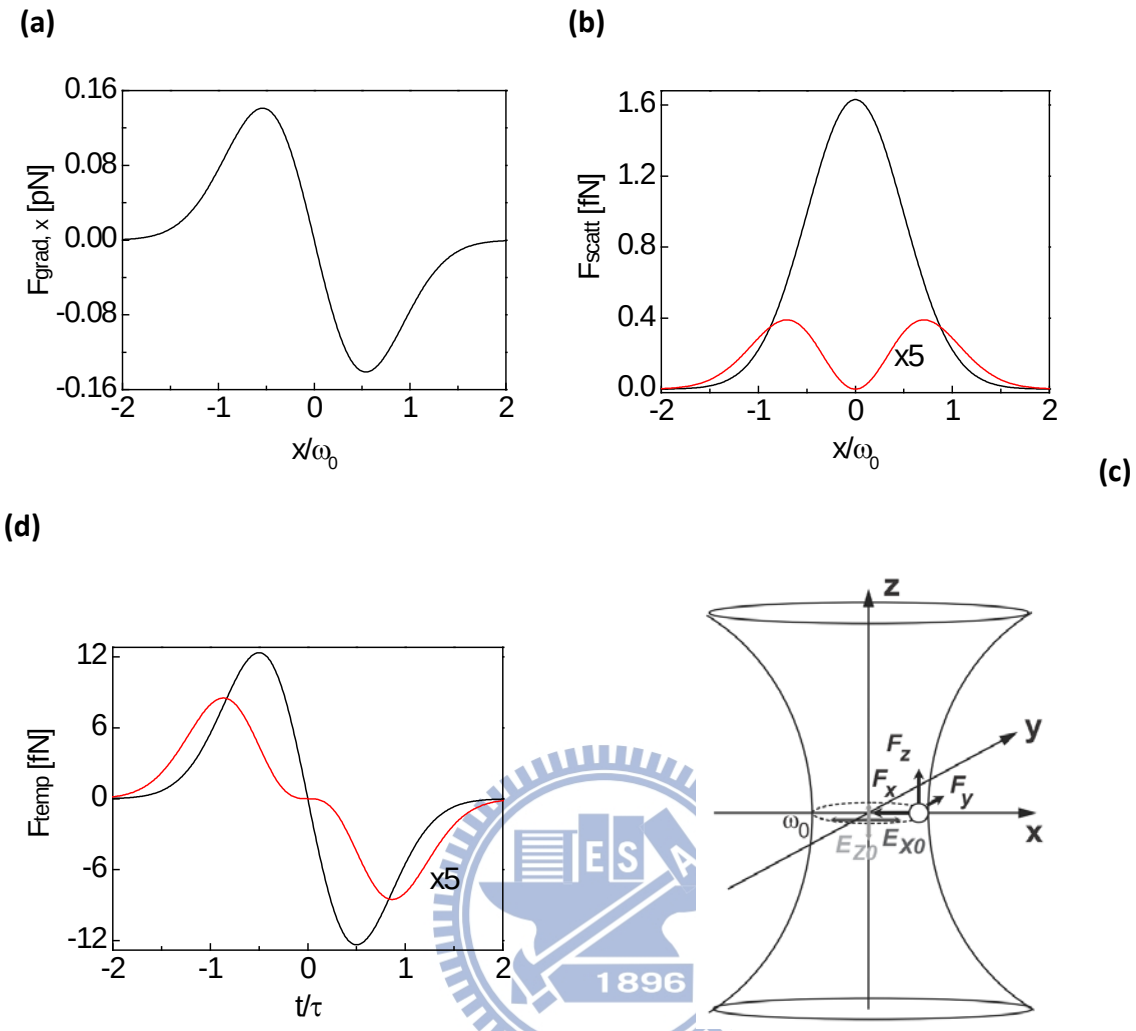

Figure 3.4 Plots of calculated gradient, scattering, and temporal forces acting on a polystyrene nanoparticle locating in the focal plane (z = 0) as a function of either the normalized lateral position of x/ω_0 or normalized time t/τ (a) Lateral component of the gradient force, F_{grad}, parallel to $\mathbf{E}_x$, at the peak of a pulse duration ($t/\tau = 0$) (b) Axial (black) and lateral (red) components of the scattering force, F_{scatt}, at the peak of a pulse duration ($t/\tau = 0$) (c) Axial (black) and lateral (red) components of the temporal force, F_{temp}. Note: for the sake of clarity, the lateral components of the scattering and temporal forces have been multiplied by a factor of 5. (d) A schematic illustration of the gradient, scattering, and temporal forces. Note; $\mathbf{F}_x = \mathbf{F}_{grad}$, $\mathbf{F}_y = F_{tempt}\hat{y} + F_{scatt}\hat{y}$, $\mathbf{F}_z = F_{tempt}\hat{z} + F_{scatt}\hat{z}$.

5. Summary

We have presented optical trapping behavior of 50-nm sized dielectric spherical nanoparticles by the tightly focused ultrashort laser pulses. In addition to the single optical trap at the focal spot, the nanoparticles were also scattered from the focus spot to the surrounding area forming a partially opened folding fan-shaped bright locus in two opposite directions, in an alternating manner, perpendicular to the laser polarization. We have shown that as compared with the cw mode, the laser pulses can confine a larger number of the Rayleigh dielectric particles around the focal spot, highlighting the impulsive peak power of the ultrashort laser pulses. The temporal forces of the laser pulses, in addition to the scattering forces, readily push the nanoparticles out of the focal spot. In particular, the lateral scattering and temporal forces, which arise from the axial component of the electric field produced by the high numerical aperture of objective lens, can control the nanoparticle flows from the focal spot to the surrounding area. The controllable directions of the scattered nanoparticles by the polarization of laser pulses will open a new vista for controlling dynamical motion of nanoparticle assembly as well as for separation and sorting of nanoparticles with either different polarizabilities or scattering cross sections.

6. References

[1] M.M. Martin, P. Plaza, N.D. Hung, Y.H. Meyer, Ultrashort pulse generation from the sweeping oscillator dye laser, in: E. Klose, B. Wilhelmi (Eds.), Ultrafast Processes in Spectroscopy, Springer-Verlag, Berlin, 1990.

[2] M.M. Martin, P. Plaza, Y.H. Meyer, J. Phys. Chem. 95 (1991) 9310.

[3] P. Plaza, M.M. Martin, Y.H. Meyer, M. Vogel, W. Rettig, Chem. Phys. 168 (1992) 365.

[4] M.M. Martin, P. Plaza, Y.H. Meyer, Chem. Phys. 192 (1995) 367.

[5] P. Changenet, H. Zang, M.J. van der Meer, M. Glasbeek, P. Plaza, M.M. Martin, J. Phys. Chem. A 102 (1998) 6716.

[6] P. Changenet-Barret, C. Loukou, C. Ley, F. Lacombat, P. Plaza, J.-M. Mallet, M.M. Martin, Phys. Chem. Chem. Phys. 12 (2010) 13715.

[7] J. Brazard, A. Usman, F. Lacombat, C. Ley, M.M. Martin, P. Plaza, L. Mony, M. Heijde, G. Zabulon, C. Bowler, J. Am. Chem. Soc. 132 (2010) 4935.

[8] A. Ashkin, J.M. Dziedzic, J. Bjorkholm, S. Chu, Opt. Lett. 11 (1986) 288.

[9] A. Ashkin, Proc. Natl. Acad. Sci. U. S. A. 94 (1997) 4853.

[10] P. Bartlett, S. Henderson, J. Phys.: Condens. Matter 14 (2002) 7757.

[11] S. Joudkazis, N. Mukai, R. Wakaki, A. Yamaguchi, S. Matsuo, H. Misawa, Nature 408 (2000) 178.

[12] H. Yoshikawa, T. Matsui, H. Masuhara, Phys. Rev. E 70 (2004) 061406.

[13] P. Borowicz, J. Hotta, K. Sasaki, H. Masuhara, J. Phys. Chem. B 101 (1997) 5900.

[14] J. Hofkens, J. Hotta, K. Sasaki, H. Masuhara, T. Taniguchi, T. Miyashita, J. Am. Chem. Soc. 119 (1997) 2741.

[15] T. Sugiyama, T. Adachi, H. Masuhara, Chem. Lett. 36 (2007) 1480.

[16] Y. Tsuboi, T. Shoji, N. Kitamura, J. Phys. Chem. C 114 (2010) 5589.

[17] K. Yuyama, T. Sugiyama, H. Masuhara, J. Phys. Chem. Lett. 1 (2010) 1321.

[18] T. Rungsimanon, K. Yuyama, T. Sugiyama, H. Masuhara, Cryst. Growth Des. 10 (2010) 4686.

[19] T. Rungsimanon, K. Yuyama, T. Sugiyama, H. Masuhara, N. Tohnai, M. Miyata, J. Phys. Chem. Lett. 1 (2010) 599.

[20] I.I. Smalyukh, J. Butler, J.D. Shrout, M.R. Parsek, G.C.L. Wong, Phys. Rev. E 78 (2008) 030701.

[21] K.C. Neuman, S.M. Block, Rev. Sci. Instrum. 75 (2004) 2787.

[22] M.A. van Dijk, L.C. Kapitein, J. van Memeren, C.F. Schmidt, E.J.G. Peterman, J. Phys. Chem. B 108 (2004) 6479.

[23] B. Agate, C.T.A. Brown, W. Sibbett, K. Dholakia, Opt. Express 12 (2004) 3011.

[24] L. Pan, A. Ishikawa, N. Tamai, Phys. Rev. B 75 (2007) 161305.

[25] M. Sanz, R. de Nalda, J.F. Marco, J.G. Izquierdo, L. Banares, M. Castillejo, J. Phys.

Chem. C 114 (2010) 4864.
[26] Y. Jiang, T. Narushima, H. Okamoto, Nat. Phys. 6 (2010) 1005.
[27] Y. Jiang, C. Ma, I. Oh, Y. Hosokawa, H. Masuhara, Mod. Phys. Lett. B 24 (2010) 1739.
[28] Y. Harada, T. Asakura, Opt. Commun. 124 (1996) 529.
[29] C.F. Bohren, D.R. Huffman, Absorption and Scattering of Light by Small Particles, Wiley, New York, 1983.
[30] R.E.H. Miles, S. Rudic, A.J. Orr-Ewing, J.P. Reid, J. Phys. Chem. A 114 (2010), 7077.
[31] T. Uwada, T. Sugiyama, H. Masuhara, J. Photochem. Photobiol. A: Chem. 221 (2011) 187.
[32] P. Zemanek, A. Jonaˇs, L. ˇSramek, M. Liˇska, Opt. Lett. 24 (1999) 1448.
[33] F. Qin, Y. Liu, Z.-Y. Li, J. Opt. 12 (2010) 035209.
[34] M.J. Bloemer, J.W. Haus, P.R. Ashley, J. Opt. Soc. Am. B 7 (1990) 790.
[35] K. Sasaki, M. Tsukima, H. Masuhara, Appl. Phys. Lett. 71 (1997) 37.
[36] J.P. Gordon, Phys. Rev. A 8 (1973) 14.
[37] L.-G. Wang, C.-L. Zhao, Opt. Express 15 (2007) 10615.
[38] J.C. Shane, M. Mazilu, W.M. Lee, K. Dholakia, Opt. Express 18 (2010) 7554.
[39] C. Hosokawa, H. Yoshikawa, H. Masuhara, Phys. Rev. E 72 (2005) 021408.
[40] L.-G. Wang, H.-S. Chai, Opt. Express 19 (2011) 14389.
[41] L.W. Davis, Phys. Rev. A 19 (1979) 1177.
[42] M. Koshioka, K. Sasaki, H. Masuhara, Appl. Spectrosc. 49 (1995) 224.
[43] L. Novotny, B. Hecht, Principles of Nano-optics, Cambridge Univ. Press, United Kingdom, 2006.
[44] A. Vogel, J. Noack, G. Huttman, G. Paltauf, Appl. Phys. B 81 (2005) 1015.
[45] A. Vogel, V. Venugopalan, Chem. Rev. 103 (2003) 577.
[46] Y. Hosokawa, H. Takabayashi, S. Miura, C. Shukunami, Y. Hiraki, H. Masuhara, Appl. Phys. A 79 (2004) 795.
[47] Y. Hosokawa, M. Hagiyama, T. Iino, Y. Murakami, A. Ito, Proc. Natl. Acad. Sci. U. S. A. 108 (2011) 1777.
[48] P.-O. Gendron, F. Avaltroni, K.J. Wilkinson, J. Fluoresc. 18 (2008), 1093.

CHAPTER 4

Conclusion and Future Outlook

In this thesis, we have studied the optical trapping behaviors of micro-sized liquid crystal droplet by tightly focused cw laser beam and nano-sized polystyrene beads by femtosecond pulse-mode laser beam. One of the key findings in this thesis is the optical trapping of individual radial symmetric liquid crystalline micro-droplets is indeed followed by a molecular reconfiguration, when the laser tapping power is above a definite threshold level. This novel phenomenon is theoretically explained based upon the proposed mechanism that the molecular reconfiguration inside the droplet involves local optical reorientation at focal volume when the interaction energy of liquid crystals with dielectric anisotropy aligned by the electric field of the focused laser beam exceeds Frank distortional energy. The relevance of this mechanism is supported by the dependence of threshold power on the droplet size.

The other key findings are the high optical efficiency of laser pulses on Rayleigh nanoparticles and the laser pulse-induced nanoparticles flows out of the focal spot in two opposite directions, in an alternating manner, controlled by the laser polarization. We have successfully interpreted this novel and fascinating phenomenon based upon interaction between the polarization and the transient axial and lateral fields produced by high numerical aperture objective lens. Impulsive peak power of the ultrashort laser pulses induces ejecting forces that overcome transient restoring forces perpendicular to the incident laser polarization, pushing the nanoparticles away from the trapping site. The repetitive trapping and releasing behavior is also considered to be important advantages of pulse- over continuous wave-mode

laser beam for future optical trapping applications of Rayleigh nanoparticles.

The key findings of the novel phenomena obtained in the current research works in this thesis have provided several new vistas and future outlooks in the field of optical trapping, including the control over the molecular reordering and reconfiguration of micro-droplets by the cw laser trapping as well as control over dynamical motion of nanoparticle assembly by ultrafast laser pulses. To realize such focused laser controlling of the molecular reordering and reconfiguration as well as dynamical motion of nanoparticle assembly, some research works extending the present works in this thesis, such as changing the target materials, different particle sizes, pulse duration, repetition rate, and other combined spectroscopic measurements would be of interest to be carried out in near future.